



MIT Open Access Articles

Kalman Filtering for Attitude and Parameter Estimation of Nanosatellites Without Gyroscopes

The MIT Faculty has made this article openly available. **Please share** how this access benefits you. Your story matters.

As Published	10.2514/1.G002649
Publisher	American Institute of Aeronautics and Astronautics (AIAA)
Version	Original manuscript
Citable link	https://hdl.handle.net/1721.1/134997
Terms of Use	Creative Commons Attribution-Noncommercial-Share Alike
Detailed Terms	http://creativecommons.org/licenses/by-nc-sa/4.0/



Kalman Filtering for Attitude and Parameter Estimation of Nanosatellites without Gyroscopes

Journal:	<i>Journal of Guidance, Control, and Dynamics</i>
Manuscript ID	2016-12-G002649.R1
Manuscript Type:	Full Paper
Date Submitted by the Author:	n/a
Complete List of Authors:	Yoon, Hyosang; Massachusetts Institute of Technology, Department of Aeronautics and Astronautics Riesing, Kathleen; Massachusetts Institute of Technology, Department of Aeronautics and Astronautics Cahoy, Kerri; MIT , Aeronautics and Astronautics
Subject Index Category:	33300 Spacecraft Guidance and Control < 30000 GUIDANCE, CONTROL, AND DYNAMICS TECHNOLOGY, 33400 State Estimation < 30000 GUIDANCE, CONTROL, AND DYNAMICS TECHNOLOGY
Note: The following files were submitted by the author along with the article. You may review these files online, if you wish. Acceptance for publication will be based solely on the content of the article.	
JGCD_Yoon_R1_LaTeX.zip	

SCHOLARONE™
Manuscripts

Kalman Filtering for Attitude and Parameter Estimation of Nanosatellites without Gyroscopes

Hyosang Yoon¹, Kathleen M. Riesing² and Kerri Cahoy³
Massachusetts Institute of Technology, Cambridge, MA, 02139

In this work, a Kalman filtering algorithm is proposed that estimates the spacecraft attitude and attitude parameters without gyroscope measurements for nanosatellites. The attitude parameters include sensor and actuator alignment, spacecraft body moment of inertia, reaction wheel moment of inertia, reaction wheel speed, and the dipole moment of the spacecraft. The new filtering formulation is based on the differential form of the rigid-body rotational dynamics, so the body rate and the other attitude parameters can be updated directly by attitude measurements such that the gyroscope reading is not required. The new filter is derived in a closed form for implementation, and physical and mathematical approaches toward achieving convergence and stability with this filter are discussed. A detailed simulation is presented that demonstrates the utility of the proposed algorithm for three different types of unmodeled disturbance torques.

¹ Doctor of Philosophy Candidate, MIT Department of Aeronautics and Astronautics, 77 Massachusetts Avenue, AIAA Student Member
² Doctor of Philosophy Candidate, MIT Department of Aeronautics and Astronautics, 77 Massachusetts Avenue, AIAA Student Member
³ Associate Professor, MIT Department of Aeronautics and Astronautics, 77 Massachusetts Avenue

Nomenclature

J	= moment of inertia of a satellite (3×3 matrix)
\vec{J}	= $[J_{xx} \ J_{yy} \ J_{zz} \ J_{xy} \ J_{xz} \ J_{yz}]^T$
$\vec{\omega}$	= body rotation rate of a satellite in body frame (3×1 vector)
n	= the number of reaction wheels
j_i	= moment of inertia of the i -th reaction wheel
\vec{J}_{rw}	= $[j_1 \ j_2 \ \cdots \ j_n]^T$
ω_i	= rotation speed of the i -th reaction wheel
$\vec{\omega}_{rw}$	= $[\omega_1 \ \omega_2 \ \cdots \ \omega_n]^T$
\bar{q}	= attitude quaternion from an inertial frame to body frame
Δt	= time step
$\hat{(\cdot)}$	= estimates of (\cdot)
$\tilde{(\cdot)}$	= measurements of (\cdot)
$D(\vec{v})$	= $\text{diag}(\vec{v})$
$\text{vec}(\bar{q})$	= $[q_1 \ q_2 \ q_3]$, the vector part of a quaternion $\bar{q} = [q_1 \ q_2 \ q_3 \ q_4]^T$
I	= identity matrix

I. Introduction

In spacecraft attitude determination (AD), the Kalman filtering (KF) approach has been used for decades to fuse different types of sensor data and calculate the optimal attitude estimates. Most prior art is based on the 6-state multiplicative extended Kalman filter (MEKF) formulation that was proposed by Lefferts *et al.* [1]. One key attribute of the 6-state MEKF is that it substitutes gyroscope measurements in place of the rotational dynamics. Instead of augmenting the body rates in the KF state and propagating it with the rotational dynamics, the 6-state MEKF uses gyroscope measurement models to determine the body rates and to propagate the attitude. This approach has been widely used in real-time onboard spacecraft AD because it is not subject to the uncertainties in attitude dynamic parameters, actuator models, and external disturbances. While the 6-state MEKF does not outperform an attitude estimation KF using rotational dynamics in terms of optimality

in theory, in practice reducing the number of the unknown parameters in the system equations is preferable to make the estimator robust and stable. Additionally, modern gyroscopes such as the fiber optic gyroscope (FOG) and the hemispherical resonator gyroscope (HRG) show good performances in small form factors, so there has been little need to incorporate the rotational dynamics in the filtering formulation and to deal with the uncertainties in the dynamic parameters for traditional spacecraft.

However, the emergence of nanosatellites has motivated new filtering approaches such as that presented here, since they differ from larger satellites in some important respects. Since 2000, CubeSats have emerged as a standard form of a small satellite with widespread adoption partially due to the low-cost access to space via rideshare launch opportunities. One Unit (U) of a CubeSat is defined by $10 \times 10 \times 10 \text{ cm}^3$ with mass of less than 1.33 kg per 1U [2]. CubeSats have become a standard for university-level research as well as small satellite constellations [3, 4]. Compared to larger satellites, AD is challenging for nanosatellites due to small size and sensor availability. One of the most accurate sensors for spacecraft attitude is the star tracker. Star tracker performance depends on the aperture area and the detector size. On larger spacecraft, star trackers and gyroscopes are the core AD sensors. FOGs are widely used in commercial satellites due to their high performance and compact size. However, in spite of their compact size, FOG are still too big and expensive for nanosatellite platforms. Therefore, a CubeSat normally utilizes small micro-electro-mechanical systems (MEMS) gyroscope to measure its rotation rates. The MEMS gyroscopes are $10\text{-}100\times$ worse than the FOGs in terms of the angular random walk noise and their bias drifts much more due to temperature [5]. For this reason, precision pointing CubeSats tend not to use MEMS gyroscope measurements and solely rely on star trackers for both attitude and rate estimation when high attitude control accuracy is needed [6–8]. In this case, the 6-state MEKF based filtering formulation cannot be used and the rotational dynamics should be incorporated into the filtering formulation. This means that we must extend the filtering formulation to handle the uncertainties of the unknown attitude and actuator parameters as well.

The unknown parameters that need to be estimated include sensor and actuator alignment, spacecraft moment of inertia (MOI), spacecraft residual dipole moments, and actuator MOI if

momentum-conserving actuators are used. For the on-orbit sensor alignment calibration, both least squares (LS), or batch, estimation techniques and KF approaches are proposed in the literature [9–13]. LS techniques assume that all the data are downloaded to the ground and processed at once, while the KF approaches inherently process the data sequentially, which is more suitable for on-board processor implementations. In the KF approaches, the 6-state MEKF formulation gives the base platform of the estimator, and the misalignment parameters are augmented as additional states [11, 12].

For MOI and other attitude parameter calibration, there are two general approaches in the literature. The first approach is adaptive control. The goal of parameter calibration is to improve attitude control (AC) accuracy. Adaptive control approaches can compensate for the effect of control errors from the parameter uncertainty [14–17]. The other general approach uses estimation techniques such as LS and Kalman filtering to estimate the MOI directly, along with the actuator parameters such as misalignments and scale error [18–23]. Psiaki uses the extended Kalman filter (EKF) and nonlinear smoother in Ref. [19, 20] with only magnetometers to estimate the MOI and the other attitude parameters (excluding actuator parameters). Psiaki develops an attitude dynamics parameter estimator that includes actuator parameters with LS approaches [21]. Fosbury and Nebelecky derived an EKF formulation to estimate the actuator alignment [22], and Norman *et al.* developed a momentum-based estimation scheme for MOI and actuator alignments [23]. However, the three studies assume the use of gyroscope measurements, and accurate gyroscope measurements are generally not available for nanosatellites.

In this study, we propose a Kalman filtering approach to estimate the spacecraft attitude and body rate, as well as other parameters including spacecraft body MOI, actuator MOI, actuator and sensor misalignments, and residual dipole moment. The proposed Kalman filter, called the Attitude Parameter calibration Kalman Filter (APKF), is not a momentum-based attitude parameter estimation and only uses star tracker measurements and reaction wheel speed readings. Since the APKF does not require gyroscope measurements and is based on the EKF, it is easily applicable to nanosatellite attitude determination even for real-time onboard AD.

The outline of this paper is as follows: Section II defines the notation and framework used in this

paper. Section III discusses the attitude dynamics combined with the reaction wheels. Section IV presents our mathematical models of reaction wheels and star trackers, and Section V derives the APKF. Section VI introduces the physical and mathematical approaches for the implementation of the APKF that help keep the filter stable and converging. Section VII demonstrates the APKF's performance using simulations, and Section VIII captures conclusions.

II. Notation

The section briefly defines the mathematical notations for quaternion and vector operations that are used to describe attitude kinematics and attitude dynamics in the following sections. A 3 dimensional vector \vec{v} is defined as

$$\vec{v} = \begin{bmatrix} v_1 & v_2 & v_3 \end{bmatrix}^T \quad (1)$$

and a quaternion \bar{q} is defined as

$$\bar{q} = \begin{bmatrix} q_1 & q_2 & q_3 & q_4 \end{bmatrix}^T = \begin{bmatrix} \vec{q} \\ q_4 \end{bmatrix} \quad (2)$$

where \vec{q} is called the vector part and q_4 is called scalar term. In this study, the attitude is represented by the quaternion defined as (2) where

$$\vec{q} = \hat{e} \sin(\theta/2), \quad q_4 = \cos(\theta/2) \quad (3)$$

The unit vector \hat{e} is the axis of rotation and θ is the angle of rotation. So, the attitude quaternion always satisfies the unity norm constraint

$$\bar{q}^T \bar{q} = 1 \quad (4)$$

Vectors will be denoted by an arrow, and quaternions by an overbar in this paper. Let \bar{p} , \bar{q} , and \bar{r} be quaternions and let T_p , T_q , and T_r be corresponding direction cosine matrices (DCM). The quaternion product operator \otimes is defined such that

$$\bar{r} = \bar{p} \otimes \bar{q} = [\bar{p} \otimes] \bar{q} = \begin{bmatrix} p_4 & p_3 & -p_2 & p_1 \\ -p_3 & p_4 & p_1 & p_2 \\ p_2 & -p_1 & p_4 & p_3 \\ -p_1 & -p_2 & -p_3 & p_4 \end{bmatrix} \begin{bmatrix} q_1 \\ q_2 \\ q_3 \\ q_4 \end{bmatrix} \quad (5)$$

Thus, $\bar{r} = \bar{p} \otimes \bar{q}$ corresponds to the product $T_r = T_p T_q$.

The skew symmetric matrix that satisfies the cross product $\vec{v} \times \vec{b} = [\vec{v} \times] \vec{b}$ is given as

$$[\vec{v} \times] = \begin{bmatrix} 0 & -v_3 & v_2 \\ v_3 & 0 & -v_1 \\ -v_2 & v_1 & 0 \end{bmatrix} \quad (6)$$

for a given 3 dimensional vector \vec{v} . Using the notations defined above, a DCM corresponding to an attitude quaternion \bar{q} can be calculated as

$$A(\bar{q}) = (|q_4|^2 - |\vec{q}|^2)I_{3 \times 3} + 2\vec{q}\vec{q}^T - 2q_4[\vec{q} \times] \quad (7)$$

$A(\bar{q})$ denotes the DCM corresponding to \bar{q} in this document. From (7), it can be inferred that both \bar{q} and $-\bar{q}$ represent a same DCM. This means $\bar{q} = -\bar{q}$ in the sense of rotation.

The inverse quaternion \bar{q}^{-1} of a quaternion \bar{q} is defined as a quaternion that satisfies

$$\bar{q}^{-1} \otimes \bar{q} = \bar{q} \otimes \bar{q}^{-1} = \begin{bmatrix} 0 & 0 & 0 & 1 \end{bmatrix}^T \quad (8)$$

From (2), (7), and (8), the inverse quaternion \bar{q}^{-1} can be obtained as

$$\bar{q}^{-1} = \begin{bmatrix} -\vec{q} \\ q_4 \end{bmatrix} \text{ or } \begin{bmatrix} \vec{q} \\ -q_4 \end{bmatrix} \quad (9)$$

III. System Dynamics

The time derivative of the attitude quaternion is given as:

$$\dot{\bar{q}} = \frac{1}{2} \begin{bmatrix} \vec{\omega} \\ 0 \end{bmatrix} \otimes \bar{q} \quad (10)$$

and it is the system dynamics for the attitude quaternion in the APKF, similar to the basic six-state attitude estimation filter (BAKF) [1, 11]. Regarding the angular rates of the spacecraft body, unlike the BAKF that uses the gyroscope model as a part of the system dynamics, the APKF needs to estimate the angular rate as one of its states. This study assumes the spacecraft as a rigid body, so the rigid body dynamics, which is often referred to as *Euler's rotation equations* or *Euler's equation*, should be used as the system dynamics.

Let us consider reaction wheels (RWs) as the primary attitude actuators and divide the spacecraft into two parts: RWs and the rest of the body. The total angular momentum of the spacecraft can be written as:

$$\vec{H} = \vec{H}_a + \vec{H}_b \quad (11)$$

where \vec{H} , \vec{H}_a , and \vec{H}_b are the total, actuator and body angular momentum, respectively, in the body frame, and they are given as:

$$\vec{H}_a = \vec{H}_{rw} + J_a \vec{\omega} \quad (12)$$

$$\vec{H}_b = J_b \vec{\omega} \quad (13)$$

where \vec{H}_{rw} is the RW angular momentum from spinning about their axes, J_a is the 3×3 MOI matrix of the RWs in the body frame, and J_b is the MOI of the spacecraft body except for the RWs. The rotational dynamics of the spacecraft body only can be written as

$$\begin{aligned} \dot{\vec{H}}_b|_{Inertial} &= \vec{T}_{a2b} + \vec{T}_{ext} \\ &= \dot{\vec{H}}_b|_{Body} + \vec{\omega} \times \vec{H}_b \\ &= J_b \dot{\vec{\omega}} + \vec{\omega} \times J_b \vec{\omega} \end{aligned} \quad (14)$$

where \vec{T}_{a2b} is the *internal* torque from RWs to the body and \vec{T}_{ext} models the external torques such as gravity gradient torque and aerodynamic drag torque. The rotational dynamics for the RWs is given as:

$$\begin{aligned} \dot{\vec{H}}_a|_{Inertial} &= \vec{T}_{b2a} = \dot{\vec{H}}_a|_{Body} + \vec{\omega} \times \vec{H}_a \\ &= \dot{\vec{H}}_{rw} + J_a \dot{\vec{\omega}} + \vec{\omega} \times (\vec{H}_{rw} + J_a \vec{\omega}) \\ &= -\vec{T}_{rw} + J_a \dot{\vec{\omega}} + \vec{\omega} \times (\vec{H}_{rw} + J_a \vec{\omega}) \end{aligned} \quad (15)$$

where \vec{T}_{a2b} is the reaction torque from the body to RWs, $\vec{T}_{b2a} = -\vec{T}_{a2b}$ and $\vec{T}_{rw} = -\dot{\vec{H}}_{rw}$ is the reaction torque due to change in speed of the RWs. Combining (14) and (15),

$$J \dot{\vec{\omega}} = -\vec{\omega} \times (J \vec{\omega} + \vec{H}_{rw}) + \vec{T}_{rw} + \vec{T}_{ext} \quad (16)$$

where $J = J_a + J_b$. Eq. (16) is the time derivative equation of the body rate $\vec{\omega}$ and will be used as the system dynamics equation for the propagation of state and covariance.

IV. Actuator and Sensor Models

A. Reaction Wheels

The reaction wheel model is important because of \vec{H}_{rw} and \vec{T}_{rw} in Eq. (16). Let us consider the RW model whose rotation axis is fixed in the body frame with a constant rotor MOI. The angular momentum of RWs in body frame is given as:

$$\begin{aligned}\vec{H}_{rw} &= j_1 \begin{bmatrix} c_{11} \\ c_{21} \\ c_{31} \end{bmatrix} \omega_1 + j_2 \begin{bmatrix} c_{12} \\ c_{22} \\ c_{32} \end{bmatrix} \omega_2 + \cdots + j_n \begin{bmatrix} c_{1n} \\ c_{2n} \\ c_{3n} \end{bmatrix} \omega_n \\ &= j_1 \vec{c}_1 \omega_1 + j_2 \vec{c}_2 \omega_2 + \cdots + j_n \vec{c}_n \omega_n\end{aligned}\quad (17)$$

where j_i , \vec{c}_i , and ω_i are the MOI, the rotation axis vector, and the rotation speed of the i -th reaction wheel respectively, and n is the number of the reaction wheels in the reaction wheel assembly (RWA). Since the rotation axis only contains directional information, it has the unity norm constraint as:

$$|\vec{c}_i| = 1 \quad (18)$$

Eq. (17) can be expressed in a matrix form as:

$$\begin{aligned}\vec{H}_{rw} &= \underbrace{\begin{bmatrix} c_{11} & c_{12} & \cdots & c_{1n} \\ c_{21} & c_{22} & \cdots & c_{2n} \\ c_{31} & c_{32} & \cdots & c_{3n} \end{bmatrix}}_{C_{rw}} \underbrace{\begin{bmatrix} j_1 & 0 & \cdots & 0 \\ 0 & j_2 & \ddots & \vdots \\ \vdots & \ddots & \ddots & 0 \\ 0 & \cdots & 0 & j_n \end{bmatrix}}_{J_{rw}} \begin{bmatrix} \omega_1 \\ \omega_2 \\ \vdots \\ \omega_n \end{bmatrix} \\ &= C_{rw} J_{rw} \vec{\omega}_{rw}\end{aligned}\quad (19)$$

By definition, the *reaction* torque of the RWA is given as:

$$\vec{T}_{rw} = -\dot{\vec{H}}_{rw} = -C_{rw} J_{rw} \vec{\alpha}_{rw} \quad (20)$$

where $\vec{\alpha}_{rw} = \dot{\vec{\omega}}_{rw}$. In actual reaction wheel hardware, $\vec{\omega}_{rw}$ is directly measured by Hall-effect sensors or optical encoders and $\vec{\alpha}_{rw}$ is obtained by numerical differentiation of $\vec{\omega}_{rw}$. Assuming a Gaussian RW speed read-out noise $\vec{n}_{rw} \sim N(0, R_{rw})$, the RW speed measurement $\tilde{\vec{\omega}}_{rw}$ can be modeled as:

$$\tilde{\vec{\omega}}_{rw} = \vec{\omega}_{rw} + \vec{n}_{rw} \quad (21)$$

Unlike the RW speed, there is no method to measure the RWA alignment matrix C_{rw} and the RWA MOIs J_{rw} directly on orbit. These are the parameters that need to be estimated in the APKF. The rotation axis vector C_{rw} has the unity constraint (18), so it needs careful consideration. Pittelkau has shown that the measurement vector of a gyroscope has two degrees of freedom in terms of misalignment, and derived a general gyroscope misalignment model in Ref. [24]. Reaction wheel misalignments can be modeled and linearly approximated in the same manner as:

$$\vec{c}_i \simeq \vec{c}_{i,0} + \vec{c}_{i,1}\delta_{i,1} + \vec{c}_{i,2}\delta_{i,2} \quad (22)$$

where $\vec{c}_{i,0}$ is the initial guess for the i -th RW, $\vec{c}_{i,1}$ and $\vec{c}_{i,2}$ are the two unit vectors that are orthogonal to $\vec{c}_{i,0}$, and $\delta_{i,1}$ and $\delta_{i,2}$ are the small misalignment angles. $\vec{c}_{i,1}$ and $\vec{c}_{i,2}$ can be any two vectors that satisfy

$$\vec{c}_{i,0} \perp \vec{c}_{i,1} \perp \vec{c}_{i,2}. \quad (23)$$

Strictly speaking, Eq. (22) does not exactly satisfy the unity norm constraint (18), but it is a good approximation for linear filtering approaches such as the Kalman filter. Using Eq. (22), the alignment matrix C_{rw} can be approximated as:

$$\begin{aligned} C_{rw} &\simeq \underbrace{\begin{bmatrix} \vec{c}_{1,0} & \cdots & \vec{c}_{n,0} \end{bmatrix}}_{C_{rw,0}} + \underbrace{\begin{bmatrix} \vec{c}_{1,1} & \cdots & \vec{c}_{n,1} \end{bmatrix}}_{C_{rw,1}} \begin{bmatrix} \delta_{1,1} & & 0 \\ & \ddots & \\ 0 & & \delta_{n,1} \end{bmatrix} \\ &\quad + \underbrace{\begin{bmatrix} \vec{c}_{1,2} & \cdots & \vec{c}_{n,2} \end{bmatrix}}_{C_{rw,2}} \begin{bmatrix} \delta_{1,2} & & 0 \\ & \ddots & \\ 0 & & \delta_{n,2} \end{bmatrix} \\ &= C_{rw,0} + C_{rw,1}D(\vec{\delta}_{rw,1}) + C_{rw,2}D(\vec{\delta}_{rw,2}) \end{aligned} \quad (24)$$

where

$$\begin{aligned} \vec{\delta}_{rw,1} &= \begin{bmatrix} \delta_{1,1} & \cdots & \delta_{n,1} \end{bmatrix}^T \\ \vec{\delta}_{rw,2} &= \begin{bmatrix} \delta_{1,2} & \cdots & \delta_{n,2} \end{bmatrix}^T \end{aligned} \quad (25)$$

We make an assumption for the RW acceleration that $\vec{\alpha}_{rw}$ is constant during Δt between two time steps of the filter as:

$$\vec{\alpha}_{rw} = \frac{1}{\Delta t}(\vec{\omega}_{rw}^+ - \vec{\omega}_{rw}^-) \quad (26)$$

where the superscript $-$ and $+$ means the beginning and the end of each propagation step in the Kalman filter.

B. Star Tracker Model

The APKF is assumed to use a star tracker that measures a attitude quaternion from a reference inertial frame to its sensor frame, whose mathematical model is given as

$$\bar{q}_m = {}^s\bar{q}_i = \bar{q}_n \otimes {}^s\bar{q}_b \otimes \bar{q} \quad (27)$$

where ${}^s\bar{q}_b$ is the attitude quaternion from the body frame to the sensor frame (sensor alignment) and \bar{q}_n is a noise quaternion, approximately given as:

$$\bar{q}_n \simeq \begin{bmatrix} \frac{1}{2}\vec{v}_q \\ 1 \end{bmatrix} \quad (28)$$

where

$$\vec{v}_q \sim N(0, R_q) \quad (29)$$

$$R_q = \text{diag}(\sigma_{q1}^2, \sigma_{q2}^2, \sigma_{q3}^2) \quad (30)$$

Note that the units of σ_q are radians. Since the sensor alignment quaternion ${}^s\bar{q}_b$ should be estimated along with the attitude quaternion \bar{q} , it also needs to be augmented in the state vector afterwards.

V. APKF

A. Error State Dynamics

The APKF is basically an attitude estimation Kalman filter that estimates the attitude \bar{q} . Unlike BAKF, APKF does not use a gyroscope model to determine the body rate and to propagate its attitude. Therefore, the APKF needs to estimate the body rates $\vec{\omega}$ explicitly as a part of its state vector. The dynamics for the body rate is given by Eq. (16), and we can combine it with the

reaction wheel models Eq. (17)-Eq. (26) as:

$$\dot{\vec{\omega}} = J^{-1}[-\vec{\omega} \times (J\vec{\omega} + C_{rw}J_{rw}\vec{\omega}_{rw}) - \frac{1}{\Delta t}C_{rw}J_{rw}(\vec{\omega}_{rw}^+ - \vec{\omega}_{rw}^-) + \vec{T}_{ext}] \quad (31)$$

where C_{rw} is function of the reaction wheels' misalignment angles ($\vec{\delta}_{rw,1}$ and $\vec{\delta}_{rw,2}$) with respect to its initial value $C_{rw,0}$ as Eq. (24). The external torque \vec{T}_{ext} consists of the gravity-gradient torque, magnetic torque due to body's residual dipole moment, aerodynamic torque, solar radiation torque, etc. as:

$$\vec{T}_{ext} = \vec{\tau}_g + \vec{\tau}_m + \vec{\tau}_a + \vec{\tau}_s + \vec{\tau}_{etc} \quad (32)$$

The gravity-gradient torque and the magnetic torque is given as:

$$\vec{\tau}_g = \begin{bmatrix} G_{b23}(J_{yy} - J_{zz}) + (G_{b33} - G_{b22})J_{yz} + G_{b13}J_{xy} - G_{b12}J_{xz} \\ G_{b13}(J_{zz} - J_{xx}) + (G_{b11} - G_{b33})J_{xz} + G_{b12}J_{yz} - G_{b23}J_{xy} \\ G_{b12}(J_{xx} - J_{yy}) + (G_{b22} - G_{b11})J_{xy} + G_{b23}J_{xz} - G_{b13}J_{yz} \end{bmatrix} \quad (33)$$

$$= \Psi(G_b)\vec{J} = -\Psi(J)\vec{G}_b \quad (34)$$

$$\vec{\tau}_m = \vec{m} \times \vec{b}_b \quad (35)$$

where $\vec{m} = [m_x, m_y, m_z]^T$ is the residual dipole moment of the spacecraft,

$$G_b = A(\vec{q})G_iA(\vec{q})^T \quad (36)$$

$$\vec{b}_b = A(\vec{q})\vec{b}_i \quad (37)$$

and $\Psi(G)$ is defined for a 3 by 3 symmetric matrix G as:

$$\Psi(G) = \begin{bmatrix} 0 & G_{23} & -G_{23} & G_{13} & -G_{12} & (G_{33} - G_{22}) \\ -G_{13} & 0 & G_{13} & -G_{23} & (G_{11} - G_{33}) & G_{12} \\ G_{12} & -G_{12} & 0 & (G_{22} - G_{11}) & G_{23} & -G_{13} \end{bmatrix} \quad (38)$$

G_i is the gravity-gradient tensor in inertial coordinates given by:

$$G_i = -\frac{\mu}{r^3} \left(I - 3\frac{\vec{r} \cdot \vec{r}^T}{r^2} \right) \quad (39)$$

where \vec{r} is the satellite's position in inertial frames, and \vec{b}_i is the geomagnetic field in inertial coordinates. Both are assumed to be known in this study. From this point, we regard the other

external torques except $\vec{\tau}_g$ and $\vec{\tau}_m$ as contributors to the disturbance torque $\vec{\tau}_d$ which is a bias driven by a second Gaussian white-noise process, similar to the gyro bias in Ref. [1]. It is possible to explicitly model the disturbance torques such as the aerodynamic torque and solar radiation torque in theory, but it is difficult to have consistent mathematical models for aerodynamic torque and solar radiation torque in practice since they heavily depend on a satellite's shape and solar activity level. Also, their magnitudes can be assumed to be smaller than reaction wheel control torques and the other external torques [25]. Therefore, we will use the simple bias model for the residual disturbance torques as:

$$\dot{\vec{\tau}}_d = \vec{\eta}_d \quad (40)$$

where $E[\vec{\eta}_d \vec{\eta}_d^T] = Q_d$, and set Q_d big enough to cover the un-modeled disturbance torque. This approach will be verified by numerical simulations in Sec. VII.

In Eq. (31), every term except Δt is actually unknown beyond an initial guess. The unknown parameters to be estimated along with $\vec{\omega}$ are the reaction wheel speed $\vec{\omega}_{rw}$, the disturbance torque $\vec{\tau}_d$, the MOI of the spacecraft $\vec{J} = [J_{xx}, J_{yy}, J_{zz}, J_{xy}, J_{xz}, J_{yz}]^T$, the MOI of the reaction wheels $\vec{J}_{rw} = [j_1, j_2, \dots, j_n]^T$, and the reaction wheel misalignment angles $\vec{\delta}_{rw} = [\delta_{rw,1}^T, \delta_{rw,2}^T]^T$.

To apply the extended Kalman filter (EKF), it is important to obtain the linearized dynamics of the error states. For the attitude quaternion, the time derivative of the vector part of the error quaternion $\delta \vec{q} = \vec{q} \otimes \hat{\vec{q}}^{-1}$ is given in Ref. [1] as:

$$\delta \dot{\vec{q}} = -[\hat{\vec{\omega}} \times] \delta \vec{q} + \frac{1}{2} \delta \vec{\omega} \quad (41)$$

for body rates, with the error states defined as:

$$\delta \vec{\omega} = \vec{\omega} - \hat{\vec{\omega}}$$

$$\delta \vec{\tau}_d = \vec{\tau}_d - \hat{\vec{\tau}}_d$$

$$\delta \vec{J} = \vec{J} - \hat{\vec{J}}$$

$$\delta \vec{m} = \vec{m} - \hat{\vec{m}}$$

$$\Delta \vec{\delta}_{rw} = \vec{\delta}_{rw} - \hat{\vec{\delta}}_{rw}$$

$$\delta \vec{J}_{rw} = \vec{J}_{rw} - \hat{\vec{J}}_{rw}$$

$$\begin{aligned}
\delta \vec{\omega}_{rw} &= \vec{\omega}_{rw} - \hat{\vec{\omega}}_{rw} \\
\delta \vec{\omega}_{rw}^- &= \vec{\omega}_{rw}^- - \hat{\vec{\omega}}_{rw}^- \\
\delta \vec{\omega}_{rw}^+ &= \vec{\omega}_{rw}^+ - \hat{\vec{\omega}}_{rw}^+
\end{aligned} \tag{42}$$

and the RW speed measurement model (21), Eq. (31) can be written as:

$$\begin{aligned}
\dot{\vec{\omega}} &= (I - \hat{J}^{-1} \delta J) \hat{J}^{-1} [-(\hat{\vec{\omega}} + \delta \vec{\omega}) \times \{(\hat{J} + \delta J)(\hat{\vec{\omega}} + \delta \vec{\omega}) \\
&\quad + (\hat{C}_{rw} + \delta C_{rw})(\hat{J}_{rw} + \delta J_{rw})(\hat{\vec{\omega}}_{rw} + \delta \vec{\omega}_{rw})\} \\
&\quad - \frac{1}{\Delta t} (\hat{C}_{rw} + \delta C_{rw})(\hat{J}_{rw} + \delta J_{rw})(\hat{\vec{\omega}}_{rw}^+ + \delta \vec{\omega}_{rw}^+) - (\hat{\vec{\omega}}_{rw}^- + \delta \vec{\omega}_{rw}^-)) \\
&\quad + \Psi(G_b)(\hat{\vec{J}} + \delta \vec{J}) + \vec{m} \times \vec{b}_b + \hat{\vec{\tau}}_d + \delta \vec{\tau}_d]
\end{aligned} \tag{43}$$

where

$$\hat{C}_{rw} = C_{rw,0} + C_{rw,1} D(\hat{\vec{\delta}}_{rw,1}) + C_{rw,2} D(\hat{\vec{\delta}}_{rw,2}) \tag{45}$$

and

$$\begin{aligned}
\delta C_{rw} &= C_{rw} - \hat{C}_{rw} \\
&= C_{rw,1} D(\Delta \vec{\delta}_{rw,1}) + C_{rw,2} D(\Delta \vec{\delta}_{rw,2})
\end{aligned} \tag{46}$$

Note that we used the approximation of the MOI matrix inverse as:

$$\begin{aligned}
J^{-1} &= (\hat{J} + \delta J)^{-1} = [\hat{J}(I + \hat{J}^{-1} \delta J)]^{-1} \\
&\simeq (I - \hat{J}^{-1} \delta J) \hat{J}^{-1}
\end{aligned} \tag{47}$$

The estimate of Eq. (43) is given as:

$$\dot{\vec{\omega}} = \hat{J}^{-1} [-\hat{\vec{\omega}} \times (\hat{J} \hat{\vec{\omega}} + \hat{C}_{rw} \hat{J}_{rw} \hat{\vec{\omega}}_{rw}) - \frac{1}{\Delta t} \hat{C}_{rw} \hat{J}_{rw} (\hat{\vec{\omega}}_{rw}^+ - \hat{\vec{\omega}}_{rw}^-) + \Psi(\hat{G}_b) \hat{\vec{J}} + \vec{m} \times \vec{b}_b + \hat{\vec{\tau}}_d] \tag{48}$$

where

$$\hat{G}_b = A(\hat{q}) G_b A(\hat{q})^T \tag{49}$$

$$\hat{\vec{b}}_b = A(\hat{q}) \vec{b}_b \tag{50}$$

With Eq. (43) and Eq. (48), we can derive the linearized equation for the error body rates as (see Appendix A):

$$\delta \dot{\vec{\omega}} = 2 \hat{J}^{-1} \{ \Psi(\hat{\vec{J}}) \Upsilon(\hat{\vec{G}}_b) + [\hat{\vec{m}} \times] [\hat{\vec{b}}_b \times] \} \delta \vec{q} + \hat{J}^{-1} \{ -[\hat{\vec{\omega}} \times] \hat{J} + [\hat{\vec{H}}_t \times] \} \delta \vec{\omega} + \hat{J}^{-1} \delta \vec{\tau}_d$$

$$\begin{aligned}
& +\hat{J}^{-1}\{\Psi(\hat{\vec{G}}_b) - [\hat{\vec{\omega}} \times] \Omega(\hat{\vec{\omega}}) - \Omega(\hat{J}^{-1}\hat{\vec{\tau}}_t)\}\delta\vec{J} - \hat{J}^{-1}[\hat{\vec{b}}_b \times] \delta\vec{m} \\
& +\hat{J}^{-1}\{-[\hat{\vec{\omega}} \times] C(\hat{\vec{h}}_{rw}) + C(\hat{\vec{t}}_{rw})\}\Delta\vec{\delta}_{rw} + \hat{J}^{-1}\{-[\hat{\vec{\omega}} \times] \hat{C}_{rw} D(\hat{\vec{\omega}}_{rw}) - \hat{C}_{rw} D(\hat{\vec{\alpha}}_{rw})\}\delta\vec{J}_{rw} \\
& -\hat{J}^{-1}[\hat{\vec{\omega}} \times] \hat{C}_{rw} \hat{J}_{rw} \delta\vec{\omega}_{rw} + \frac{1}{\Delta t} \hat{J}^{-1} \hat{C}_{rw} \hat{J}_{rw} \delta\vec{\omega}_{rw}^- - \frac{1}{\Delta t} \hat{J}^{-1} \hat{C}_{rw} \hat{J}_{rw} \delta\vec{\omega}_{rw}^+
\end{aligned} \tag{51}$$

where

$$\hat{\vec{h}}_{rw} = \hat{J}_{rw} \hat{\vec{\omega}}_{rw} \tag{52}$$

$$\hat{\vec{\alpha}}_{rw} = \frac{1}{\Delta t} (\hat{\vec{\omega}}_{rw}^+ - \hat{\vec{\omega}}_{rw}^-) \tag{53}$$

$$\hat{\vec{t}}_{rw} = -\hat{J}_{rw} \hat{\vec{\alpha}}_{rw} \tag{54}$$

$$\hat{\vec{H}}_t = \hat{J} \hat{\vec{\omega}} + \hat{C}_{rw} \hat{\vec{h}}_{rw} \tag{55}$$

$$\hat{\vec{\tau}}_t = -\hat{\vec{\omega}} \times \hat{\vec{H}}_t + \hat{C}_{rw} \hat{\vec{t}}_{rw} + \Psi(\hat{\vec{G}}_b) \hat{\vec{J}} + \hat{\vec{m}} \times \hat{\vec{b}}_b + \hat{\vec{\tau}}_d \tag{56}$$

matrix $C(\vec{v})$ and $\Omega(\vec{v})$ are defined for a vector \vec{v} as:

$$C(\vec{v}) = \begin{bmatrix} \vec{c}_{1,1}v_1 & \vec{c}_{2,1}v_2 & \cdots & \vec{c}_{n,1}v_n & \vec{c}_{1,2}v_1 & \vec{c}_{2,2}v_2 & \cdots & \vec{c}_{n,2}v_n \end{bmatrix} \tag{57}$$

$$\Omega(\vec{v}) = \begin{bmatrix} v_1 & 0 & 0 & v_2 & v_3 & 0 \\ 0 & v_2 & 0 & v_1 & 0 & v_3 \\ 0 & 0 & v_3 & 0 & v_1 & v_2 \end{bmatrix} \tag{58}$$

and matrix $\Upsilon(G)$ is defined for a 3 by 3 symmetric matrix as:

$$\Upsilon(\vec{G}) = \begin{bmatrix} 0 & 2\hat{G}_{13} & -2\hat{G}_{12} \\ -2\hat{G}_{23} & 0 & 2\hat{G}_{12} \\ 2\hat{G}_{23} & -2\hat{G}_{13} & 0 \\ -\hat{G}_{13} & \hat{G}_{23} & (\hat{G}_{11} - \hat{G}_{22}) \\ \hat{G}_{12} & (\hat{G}_{33} - \hat{G}_{11}) & -\hat{G}_{23} \\ (\hat{G}_{22} - \hat{G}_{33}) & -\hat{G}_{12} & \hat{G}_{13} \end{bmatrix} \tag{59}$$

\vec{J} , \vec{m} , $\vec{\delta}_{rw}$, and \vec{J}_{rw} are assumed to be constant, but we add small process noises ($\vec{\eta}_J$, $\vec{\eta}_m$, $\vec{\eta}_{\delta rw}$ and $\vec{\eta}_{Jrw}$, respectively) to deal with a small change in the values due to thermal distortion and to prevent the APKF from becoming closed.

The reaction wheel speeds, with the assumption of constant acceleration with Eq. (26), $\vec{\omega}_{rw}$ can

be written as:

$$\vec{\omega}_{rw} = \vec{\omega}_{rw}^- + \vec{\alpha}_{rw}(t - t_0) \quad (60)$$

$$\begin{aligned} \dot{\vec{\omega}}_{rw} &= \vec{\alpha}_{rw} \\ &= \frac{1}{\Delta t} [\hat{\vec{\omega}}_{rw}^+ + \delta\vec{\omega}_{rw}^+ - (\hat{\vec{\omega}}_{rw}^- + \delta\vec{\omega}_{rw}^-)] \end{aligned} \quad (61)$$

Since the estimate of Eq. (61) is given as Eq. (53),

$$\begin{aligned} \delta\dot{\vec{\omega}}_{rw} &= \dot{\vec{\omega}}_{rw} - \dot{\vec{\omega}}_{rw} \\ &= \frac{1}{\Delta t} \delta\vec{\omega}_{rw}^+ - \frac{1}{\Delta t} \delta\vec{\omega}_{rw}^- \end{aligned} \quad (62)$$

B. Relative Calibration for MOIs and Alignments

The error states in Eq. (42) include both the MOI of the spacecraft body and the MOIs of the RWs, which means there is no absolute reference we can rely on for the MOI calibration. Conceptually speaking, the attitude sensors such as star trackers measure the body rates (though it is an indirect measurement), the reaction wheels measure their rotation speed, and the filter compares those two measurements and extracts the relative ratio between the body MOI and the RW MOIs. For a simple example, consider a RW on a frictionless turntable and assume it is initially stationary. If the RW starts to rotate, the turntable will rotate in the opposite direction. Although we assume perfect measurements of the RW speed and the turntable rotation rate, the only thing we can calculate is the ratio between the MOIs of the RW and the turntable unless we know one of them *a priori*. This means that both MOIs are not observable from the two rotation rate measurements.

To resolve this observability issue, we assume J_{xx} as the reference MOI and estimate the remaining five terms $\vec{J}_5 = [J_{yy}, J_{zz}, J_{xy}, J_{xz}, J_{yz}]^T$, similar to Ref. [19]. The estimation results of \vec{J}_5 and \vec{J}_{rw} will be scaled to the ratio of the nominal and actual value of J_{xx} . The estimates of \vec{J}_5 and \vec{J}_{rw} will not converge on the actual MOI values, but this does not matter for attitude determination and control because they only use the relative ratios between the MOIs. For attitude filtering, the multiplication of J^{-1} in Eq. (31) erases the scaling error of J and J_{rw} . For attitude control, since the reaction wheel torque is typically generated by its rotation speed control, the same scaling error in the MOIs will not produce any undesired torque error.

For alignment calibration, if N sensors are used, only $N - 1$ alignments can be estimated by the sensor measurements as discussed by Pittelkau [12]. This means that the misalignments of the RW axis C_{rw} and the star tracker ${}^s\bar{q}_b$ are not fully observable at the same time with only one star tracker. Therefore, we set the star tracker's sensor frame as the reference frame, and the RWs rotation axes are estimated with respect to the star tracker frame. The misalignment of the star tracker is blended into the RW rotation axis and the body MOI. It is possible to use RWs rotation axes as the reference as Pittelkau did in Ref. [24] using gyroscopes' measurements axes, but it is not covered in this paper.

C. State Transition Matrix

With Eq. (41) and Eq. (51), the linearized time derivative equations for the error states, $\delta\bar{q}$ and Eq. (42), can be written in matrix form as:

$$\frac{d}{dt} \begin{bmatrix} \delta\bar{q} \\ \delta\vec{\omega} \\ \delta\vec{\tau}_d \\ \delta\vec{J}_5 \\ \delta\vec{m} \\ \Delta\delta_{rw} \\ \delta\vec{J}_{rw} \\ \delta\vec{\omega}_{rw} \\ \delta\vec{\omega}_{rw}^- \\ \delta\vec{\omega}_{rw}^+ \end{bmatrix} = \underbrace{\begin{bmatrix} -[\hat{\vec{\omega}} \times] & 0.5I & 0 & 0 & 0 & 0 & 0 & 0 & 0 & 0 & 0 \\ F_{21} & F_{22} & F_{23} & F_{24} & F_{25} & F_{26} & F_{27} & F_{28} & F_{29} & F_{2a} & 0 \\ & & 0 & & & & & & & & \\ & & & 0 & & & & & & & \\ & & & & 0 & & & & & & \\ & & & & & 0 & & & & & \\ & & & & & & 0 & & & & \\ & & & & & & & 0 & F_{89} & F_{8a} & \\ & & & & & & & & 0 & & \\ & & & & & & & & & 0 & \end{bmatrix}}_F \underbrace{\begin{bmatrix} \delta\bar{q} \\ \delta\vec{\omega} \\ \delta\vec{\tau}_d \\ \delta\vec{J}_5 \\ \delta\vec{m} \\ \Delta\delta_{rw} \\ \delta\vec{J}_{rw} \\ \delta\vec{\omega}_{rw} \\ \delta\vec{\omega}_{rw}^- \\ \delta\vec{\omega}_{rw}^+ \end{bmatrix}}_{\Delta\vec{x}}$$

where

$$F_{8a} = \frac{1}{\Delta t} I \quad (75)$$

and, $\Omega_5(\vec{v})$ and $\Psi_5(G)$ are defined for the 5-element MOI error state vector $\delta\vec{J}_5$ as:

$$\Omega_5(\vec{v}) = \begin{bmatrix} 0 & 0 & v_2 & v_3 & 0 \\ v_2 & 0 & v_1 & 0 & v_3 \\ 0 & v_3 & 0 & v_1 & v_2 \end{bmatrix} \quad (76)$$

$$\Psi_5(G) = \begin{bmatrix} G_{23} & -G_{23} & G_{13} & -G_{12} & (G_{33} - G_{22}) \\ 0 & G_{13} & -G_{23} & (G_{11} - G_{33}) & G_{12} \\ -G_{12} & 0 & (G_{22} - G_{11}) & G_{23} & -G_{13} \end{bmatrix} \quad (77)$$

The process noise has diagonal covariances $E[\tilde{\eta}_d \tilde{\eta}_d^T] = Q_d = \text{diag}(q_d, q_d, q_d)$, $E[\tilde{\eta}_J \tilde{\eta}_J^T] = Q_J = \text{diag}(q_{Jm}, q_{Jm}, q_{Jp}, q_{Jp}, q_{Jp})$, $E[\tilde{\eta}_m \tilde{\eta}_m^T] = Q_m = \text{diag}(q_m, q_m, q_m)$, $E[\tilde{\eta}_{\delta rw} \tilde{\eta}_{\delta rw}^T] = Q_{\delta rw} = \text{diag}(q_{\delta rw}, \dots, q_{\delta rw})$, and $E[\tilde{\eta}_{Jrw} \tilde{\eta}_{Jrw}^T] = Q_{Jrw} = \text{diag}(q_{Jrw}, \dots, q_{Jrw})$.

The state transition matrix Φ can be obtained by integrating Eq. (63) either numerically or with an analytical approximation. For the numerical method, Φ can be approximated using a Taylor series simply as:

$$\Phi_{k,k-1} = e^{F\Delta t} = I + F\Delta t + \frac{1}{2!}F^2\Delta t^2 + \frac{1}{3!}F^3\Delta t^3 + \dots \quad (78)$$

where Δt is the time step between $k - 1$ and k . This numerical method is simple and easy to implement, but computationally burdensome especially when the number of states is large. It is preferable to use a closed-form approximation of Φ , as derived in Appendix B,

$$\Phi = \begin{bmatrix} \phi_{11} & \phi_{12} & \phi_{13} & \phi_{14} & \phi_{15} & \phi_{16} & \phi_{17} & \phi_{18} & \phi_{19} & \phi_{1a} \\ \phi_{21} & \phi_{22} & \phi_{23} & \phi_{24} & \phi_{25} & \phi_{26} & \phi_{27} & \phi_{28} & \phi_{29} & \phi_{2a} \\ 0 & 0 & I & 0 & 0 & 0 & 0 & 0 & 0 & 0 \\ 0 & 0 & 0 & I & 0 & 0 & 0 & 0 & 0 & 0 \\ 0 & 0 & 0 & 0 & I & 0 & 0 & 0 & 0 & 0 \\ 0 & 0 & 0 & 0 & 0 & I & 0 & 0 & 0 & 0 \\ 0 & 0 & 0 & 0 & 0 & 0 & I & 0 & 0 & 0 \\ 0 & 0 & 0 & 0 & 0 & 0 & 0 & I & \phi_{89} & \phi_{8a} \\ 0 & 0 & 0 & 0 & 0 & 0 & 0 & 0 & I & 0 \\ 0 & 0 & 0 & 0 & 0 & 0 & 0 & 0 & 0 & I \end{bmatrix}$$

where

$$\phi_{11} = I - [\hat{\omega} \times] \Delta t \quad (79)$$

$$\phi_{12} = \frac{1}{2} \kappa_{11} \quad (80)$$

$$\phi_{1i} = \frac{1}{2} \kappa_{12} F_{2i} \quad (81)$$

$$\phi_{1j} = \frac{1}{2} \kappa_{12} F_{2j} + \frac{1}{2} \kappa_{13} F_{28} F_{8j} \quad (82)$$

$$\phi_{21} = F_{21} \Delta t + \frac{1}{2} (F_{22} F_{21} - F_{21} [\hat{\omega} \times]) \Delta t^2 - \frac{1}{6} F_{22} F_{21} [\hat{\omega} \times] \Delta t^3 \quad (83)$$

$$\phi_{22} = I + F_{22} \Delta t + \frac{1}{2} \left(\frac{1}{2} F_{21} + F_{22} F_{22} \right) \Delta t^2 \quad (84)$$

$$\phi_{2i} = \kappa_{21} F_{2i} \quad (85)$$

$$\phi_{2j} = \kappa_{21} F_{2j} + \kappa_{22} F_{28} F_{8j} \quad (86)$$

$$\phi_{8j} = F_{8j} \Delta t \quad (87)$$

for $i = 3, 4, \dots, 8$ and $j = 9, a$ where

$$\kappa_{11} = I \Delta t + \frac{1}{2} (F_{22} - [\hat{\omega} \times]) \Delta t^2 - \frac{1}{6} [\hat{\omega} \times] F_{22} \Delta t^3 \quad (88)$$

$$\kappa_{12} = \frac{1}{2} I \Delta t^2 + \frac{1}{6} (F_{22} - [\hat{\omega} \times]) \Delta t^3 - \frac{1}{24} [\hat{\omega} \times] F_{22} \Delta t^4 \quad (89)$$

$$\kappa_{13} = \frac{1}{6} I \Delta t^3 + \frac{1}{24} (F_{22} - [\hat{\omega} \times]) \Delta t^4 - \frac{1}{120} [\hat{\omega} \times] F_{22} \Delta t^5 \quad (90)$$

$$\kappa_{21} = I \Delta t + \frac{1}{2} F_{22} \Delta t^2 \quad (91)$$

$$\kappa_{22} = \frac{1}{2} I \Delta t^2 + \frac{1}{6} F_{22} \Delta t^3 \quad (92)$$

D. Process Noise

In the EKF, the covariance propagation can be calculated by:

$$P_{t_1}^- = \Phi_{t_1, t_0} P_{t_0}^+ \Phi_{t_1, t_0}^T + Q_t \quad (93)$$

where Q_t is the process noise matrix given by:

$$Q_t = \int_{t_0}^{t_1} \Phi(t_1, \tau) G(\tau) Q(\tau) G^T(\tau) \Phi^T(t_1, \tau) d\tau \quad (94)$$

With the approximated state transition matrix as:

$$\phi_{11} \simeq I \quad (95)$$

$$\phi_{12} \simeq \frac{1}{2} I \Delta t \quad (96)$$

$$\phi_{1j} \simeq 0 \quad (97)$$

$$\phi_{22} \simeq I \quad (98)$$

$$\phi_{2j} \simeq F_{2j} \Delta t \quad (99)$$

for $j = 3, 4, \dots, 8$, Eq. (94) can be integrated as:

$$Q_t = \begin{bmatrix} 0 & 0 & 0 & 0 & 0 & 0 & 0 & 0 & 0 & 0 & 0 \\ Q_{t,22} & \frac{1}{2} F_{23} Q_d \Delta t^2 & \frac{1}{2} F_{24} Q_J \Delta t^2 & \frac{1}{2} F_{25} Q_m \Delta t^2 & \frac{1}{2} F_{26} Q_{\delta rw} \Delta t^2 & \frac{1}{2} F_{27} Q_{Jrw} \Delta t^2 & 0 & 0 & 0 & 0 \\ & Q_d \Delta t & 0 & 0 & 0 & 0 & 0 & 0 & 0 & 0 \\ & & Q_J \Delta t & 0 & 0 & 0 & 0 & 0 & 0 & 0 \\ & & & Q_m \Delta t & 0 & 0 & 0 & 0 & 0 & 0 \\ & & & & Q_{\delta rw} \Delta t & 0 & 0 & 0 & 0 & 0 \\ & & & & & Q_{Jrw} \Delta t & 0 & 0 & 0 & 0 \\ & & & & & & 0 & 0 & 0 & 0 \\ & & & & & & & 0 & 0 & 0 \\ & & & & & & & & 0 & 0 \\ & & & & & & & & & 0 \end{bmatrix} \quad (100)$$

where

$$Q_{t,22} = \frac{1}{3} [F_{23} Q_d F_{23}^T + F_{24} Q_J F_{24}^T + F_{25} Q_m F_{25}^T + F_{26} Q_{\delta rw} F_{26}^T + F_{27} Q_{Jrw} F_{27}^T] \Delta t^3 \quad (101)$$

Note that only the elements in the upper triangular part is displayed here. Since Q_t is symmetric, the lower triangular part is same as the transpose of the upper triangular part.

E. Update

With the same approach to substitute a quaternion by the product of an error quaternion and its estimate $\bar{q} = \delta \bar{q} \otimes \hat{q}$, Eq. (27) can be written as:

$$\bar{q}_m = \bar{q}_n \otimes \delta^s \bar{q}_b \otimes \hat{q}_b^s \otimes \delta \bar{q} \otimes \hat{q} \quad (102)$$

Using the same approaches described in Ref. [11], the vector part of the error measurement quaternion $\delta\bar{q}_m = \bar{q}_m \otimes \hat{q}_m^{-1}$ can be approximated in a linearized form as:

$$\delta\bar{q}_m \simeq \delta^s\bar{q}_b + A(^s\hat{q}_b)\delta\bar{q} + \frac{1}{2}\vec{v}_q \quad (103)$$

As discussed in Sec. VB, the APKF does not estimate the misalignment of the star tracker $\delta^s\bar{q}_b$ by assuming that only one star tracker is used, which means $\delta^s\bar{q}_b = 0$ and $^s\hat{q}_b$ remains the same as the initial value $^s\bar{q}_{b,0}$. If more than one star tracker is used, $\delta^s\bar{q}_b$ for the extra star trackers should be augmented in the state vector and needs to be estimated. For the APKF in this paper, the linearized measurement equation is given as:

$$\delta\bar{q}_m = \underbrace{\begin{bmatrix} A(^s\hat{q}_b) & 0 & \dots & 0 \end{bmatrix}}_H \Delta\vec{x} + \frac{1}{2}\vec{v}_q \quad (104)$$

H in Eq. (104) is the measurement sensitivity matrix of the star tracker for the APKF update given as:

$$K = P^- H^T (H P^- H^T + M R M^T)^{-1} \quad (105)$$

$$\Delta\vec{x}^+ = K \delta\bar{q}_m \quad (106)$$

$$P^+ = (I - KH)P^-(I - KH)^T + K M R M^T K^T \quad (107)$$

VI. Implementation Notes

A. Calibration Maneuver

For complete observability of both MOI and alignment calibration, a set of calibration maneuvers that generates control torques and angular momentum in all directions is required, similar to the discussion for gyroscope alignment calibration in Ref. [11]. In the APKF case, all directions should include not only the three X, Y, and Z directions of the body frame, but also the null vector directions of the RW alignment matrix C_{rw} . If no torques are applied in the null vector directions, it is not possible to update the misalignments on the null vector of C_{rw} . In this study, we use three consecutive rotations in each X, Y, and Z axis as one set of the calibration maneuver. It is possible to use the other types of maneuvers such as the sinusoidal maneuver with different frequency as in Ref. [11]. However, star trackers for nanosatellites perform worse under rotation than star trackers

for bigger satellites due to their smaller aperture sizes, and even for bigger satellites, star trackers usually give their best performance when the spacecraft is not rotating. To be more applicable to real nanosatellite systems, we use three stop-and-go consecutive rotations for the calibration maneuvers. Figure 1 shows the attitude commands in terms of Euler angle for a set of calibration maneuvers.

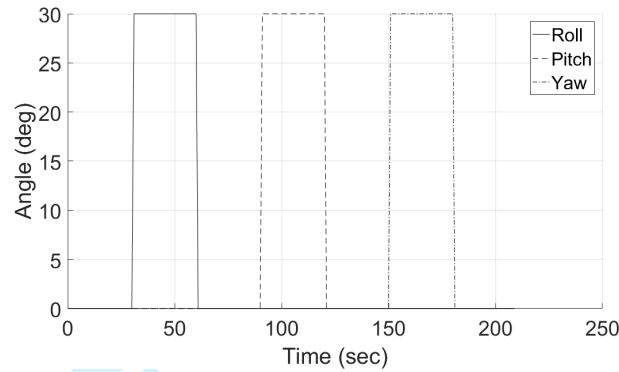


Fig. 1: A set of calibration maneuver angle commands

B. RW Torque Command

In this study, we assume the use of a quaternion feedback control law with proportional-derivative (PD) gain [26]. This PD control law gives the desired control torque, \vec{T}_c , in body frame.

To calculate the RW torque command \vec{t}_{rw} that satisfies

$$\vec{T}_c = C_{rw} \vec{t}_{rw}, \quad (108)$$

the following pseudo-inverse is usually used when the RWs are identical:

$$\vec{t}_{rw,net} = C_{rw}^T (C_{rw} C_{rw}^T)^{-1} \vec{T}_c \quad (109)$$

Eq. (109) is the efficient solution of Eq. (108) that minimizes the norm of the RW torque vector by eliminating the torque in the direction of the null space of C_{rw} which does not affect the effective control torque in the body frame. This RW torque command is good for spacecraft attitude control, but we need the RW torque in the null space of C_{rw} for the RW alignment calibration. So we add the RW torque in the null space into Eq. (109) as:

$$\vec{t}_{rw} = C_{rw}^T (C_{rw} C_{rw}^T)^{-1} \vec{T}_c + \sum_{i=1}^{n-3} a_i \vec{N}_{rw,i} \quad (110)$$

where $\vec{N}_{rw,i}$ is the i -th null vector of C_{rw} which satisfies $C_{rw}\vec{N}_{rw,i} = 0$ and a_i is the magnitude of the null torque for the i -th null vector. a_i should be determined to be small enough to avoid RW speed saturation.

C. Angular Momentum Bias

The spacecraft needs angular momentum bias to ensure complete observability of the relative MOI calibration. Let us consider a sample case where $J = \text{diag}(J_{xx}, J_{yy}, J_{zz})$ and there are only three reaction wheels that are aligned to the X, Y, and Z axes. If we assume zero total angular momentum ($J\vec{\omega} + C_{rw}J_{rw}\vec{\omega}_{rw} = 0$) and ignore the external torque \vec{T}_{ext} , the equation of motion given by Eq. (31) becomes:

$$\dot{\vec{\omega}} = \begin{bmatrix} \frac{j_1}{J_{xx}} \alpha_{rw,1} \\ \frac{j_2}{J_{yy}} \alpha_{rw,2} \\ \frac{j_3}{J_{zz}} \alpha_{rw,3} \end{bmatrix} \quad (111)$$

In Eq. (111), each axis is uncoupled with the other axes, so the relative MOI calibration to J_{xx} is not feasible. Therefore, non-zero angular momentum bias is required for the relative MOI calibration. The magnitude of the bias should be determined to be small enough to avoid RW speed saturation.

D. Variable Fictitious Noise

The APKF applies the EKF, which is a linearized estimator, to the nonlinear system. The APKF uses Eq. (63) as the system dynamics, but it is just a linearized equation, not the exact system dynamics. The discrepancy between the exact system and the linearized model may be large and may cause instability of the APKF, especially when the estimation error is large and complete observability is not obtained. In the calibration maneuver, full observability is not ensured before completing one set of the maneuvers. Once the error of the estimate becomes large compared to its estimated covariance, the error may not converge even after completing the set of calibration maneuvers. Fig. 2 shows a typical non-converging estimation result. This is the estimation result of J_{yy} of the APKF. The first set of the calibration maneuver ends at 210 sec. The estimation error becomes larger than 3σ around 140 sec and it does not converge into the 3σ boundary even after a couple of sets of the calibration maneuvers. The fundamental solution for this problem would be to

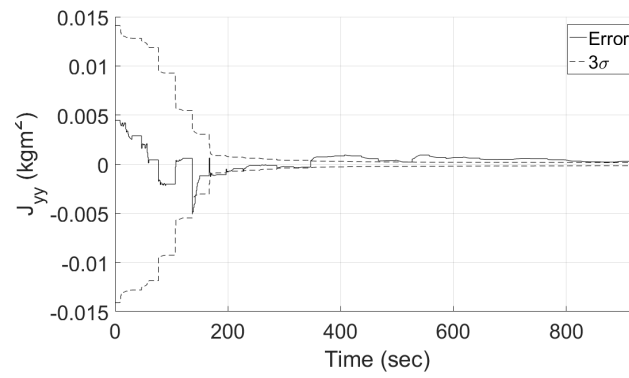


Fig. 2: Sample non-converging APKF result for J_{yy} estimates

change the filtering approach from the EKF to other nonlinear estimation techniques such as the unscented Kalman filter [27, 28] and particle filter, but they normally require intensive calculations especially when the number of states is large [29]. The APKF's state has 41 components for $n = 4$, so nonlinear filtering techniques may be too burdensome. Instead of utilizing nonlinear filters, we propose a simple strategy to mitigate this problem by varying the process and measurement noise covariances. There are five process noise vectors and one measurement noise vector, $\vec{\eta}_d, \vec{\eta}_J, \vec{\eta}_m, \vec{\eta}_{\delta rw}, \vec{\eta}_{Jrw}$, and \vec{v}_q , and the six corresponding covariance matrices, $Q_d, Q_J, Q_m, Q_{\delta rw}, Q_{Jrw}$, and R_q . The nominal values of the process noise covariances are set to be small, such as 0.1% MOI variation over one hour, since the MOIs and the alignments are assumed to be constant. On initializing the filter, we set the Q 's and R_q 100 times bigger than their nominal values to prevent the filter from becoming closed before full observability is acquired. After the first set of the calibration maneuvers, the covariance values are set to 10 times the nominal for gradual convergence, and they return to their nominal values after the second set of the calibration maneuver. With this numerical approach, the APKF gives the converging result as shown in Fig. 3 with the same inputs as used in Fig. 2. This approach does not guarantee the optimal estimation results during the transient period, but when it converges to the steady state, the non-optimality becomes negligible.

VII. Simulation Results

The following parameters for a satellite system are used to verify the APKF's performance by simulation. A typical 3U rectangular-prism CubeSat ($30 \times 10 \times 10 \text{ cm}^3$) was assumed as the

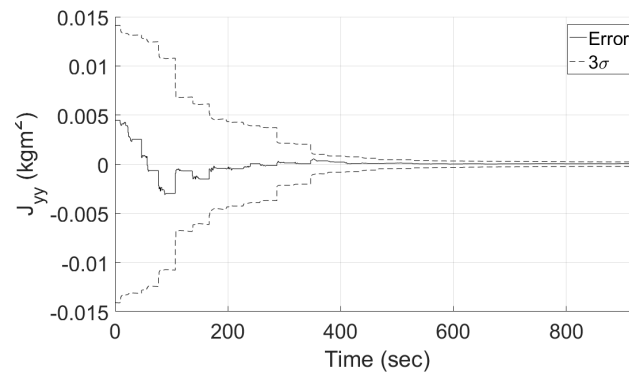


Fig. 3: Sample converging APKF result for J_{yy} estimates with variable fictitious noise

spacecraft. The nominal body MOI is $\vec{J}_0 = [12, 47, 45, 1, 2, 3]^T \times 10^{-3} \text{ kg} \cdot \text{m}^2$ and the nominal MOI of each RW is $3 \times 10^{-6} \text{ kg} \cdot \text{m}^2$. We assume that 4 RWs are used and the nominal RW rotation matrix is given as:

$$C_{rw,0} = \frac{1}{\sqrt{3}} \begin{bmatrix} -1 & -1 & 1 & 1 \\ -1 & 1 & 1 & -1 \\ 1 & 1 & 1 & 1 \end{bmatrix} \quad (112)$$

which is a symmetric pyramid configuration. The MOI errors are set to be $\pm 6\%$ to $\pm 12\%$ of its nominal value as $\Delta \vec{J} = [-1.2, 3.29, 3.6, 0.1, -0.12, 0.21]^T \times 10^{-3} \text{ kg} \cdot \text{m}^2$ and $\Delta \vec{J}_{rw} = [0.45, 0.36, -0.75, -0.60]^T \times 10^{-6} \text{ kg} \cdot \text{m}^2$. Regarding the RW misalignment, the two misalignment direction vectors $\vec{c}_{i,1}$ and $\vec{c}_{i,2}$ are calculated as:

$$\begin{aligned} \vec{c}_{i,1} &= \frac{\vec{c}_{i,0} \times \vec{c}_{i+1,0}}{|\vec{c}_{i,0} \times \vec{c}_{i+1,0}|} \\ \vec{c}_{i,2} &= \frac{\vec{c}_{i,0} \times \vec{c}_{i,1}}{|\vec{c}_{i,0} \times \vec{c}_{i,1}|} \end{aligned} \quad (113)$$

for $i = 1, 2, \dots, n$ and $\vec{c}_{n+1,0} = \vec{c}_{n,0}$. The RW alignment error angles are assumed to be $\vec{\delta}_{rw,1} = [11, -7, -11, 8]^T$ deg and $\vec{\delta}_{rw,2} = [-12, 12, 9, 10]^T$ deg, so that the actual RW rotation matrix is given as:

$$C_{rw} = \begin{bmatrix} -0.76820 & -0.72728 & 0.36636 & 0.70252 \\ -0.39087 & 0.39403 & 0.68484 & -0.59026 \\ 0.50703 & 0.56195 & 0.62988 & 0.39755 \end{bmatrix} \quad (114)$$

The RW speed read-out noise is assumed to be 10 rpm (1σ). The star tracker accuracy is assumed to be 20 arcsec (1σ) in the cross boresight axes, which are x and y axis of the body frame, and 60 arcsec (1σ) in the boresight axis, which is the z axis of the body frame. The star tracker is assumed to give output only when the magnitude of the body rate is less than 0.1 deg/sec. The residual dipole moment is assumed to be $\vec{m} = [-0.11, 0.15, 0.20]^T \text{ Am}^2$.

Regarding the attitude maneuvers, we use 5 sets of the calibration maneuver as proposed in Section VIA in this simulation. The maneuver angle and the duration for each rotation are 30 deg and 30 sec respectively, and we put 30 sec attitude-hold time before of the first set of the calibration maneuvers for the filter initialization as shown in Fig. 1. The total simulation period is 930 sec and the step time is 1 sec. The attitude, body rates, and the reaction wheel speeds are numerically integrated by the 4th order *Runge-Kutta* method. The magnitude of the null torque a_i in Eq. (110) is set to be $\pm 10\%$ of $\max(\vec{t}_{rw})$. The initial body rate is set to be $\vec{\omega}_0 = [1, 0, 0]^T \text{ deg/sec}$ to give the momentum bias for complete observability.

The nominal process noise for the MOIs, the dipole moment, and the misalignments is set to be $q_{J_m} = (4.7 \cdot 10^{-5} \text{ kgm}^2/\sqrt{\text{hr}})^2$, $q_{J_p} = (4.7 \cdot 10^{-6} \text{ kgm}^2/\sqrt{\text{hr}})^2$, $q_m = (1 \cdot 10^{-3} \text{ Am}^2/\sqrt{\text{hr}})^2$, $q_{\delta_{rw}} = (0.01 \text{ deg}/\sqrt{\text{hr}})^2$, and $q_{J_{rw}} = (3 \cdot 10^{-9} \text{ kgm}^2/\sqrt{\text{hr}})^2$.

Regarding the initialization of the APKF, the initial attitude quaternion determined by one star tracker output and the initial body rate are estimated by numerical differentiation of two star tracker outputs at the first two steps. The initial covariances (P_0) for attitude and the body rate are set to be large enough to fully cover the expected initial errors as $(10 \text{ deg})^2$ and $(10 \text{ deg/sec})^2$ respectively. The initial RW speed is determined by the RW speed reading and its P_0 is the same as the covariance of the read-out noise R_{rw} . The initial values for the other states are set to be zero. The P_0 is $(5.0 \cdot 10^{-3} \text{ kgm}^2)^2$ for J_{yy} and J_{zz} is which is 10.6% of the largest nominal body MOI value, $(2.0 \cdot 10^{-3} \text{ kgm}^2)^2$ for J_{xy} , J_{xz} , and J_{yz} , $(0.3 \text{ Am}^2)^2$ for the residual dipole moment, $(10 \text{ deg})^2$ for RW misalignments, and $(1 \cdot 10^{-6} \text{ kgm}^2)^2$ for RW MOIs.

We present three sets of simulation results with different unmodeled disturbance torques. The first simulation is performed with zero disturbance torques to verify the convergence of the APKF itself (Case 1), and the second simulation is performed with sinusoidal disturbance torques to ex-

amine its stability for unmodeled disturbances (Case 2). The comparison of the results of Case 1 to Case 2 shows performance degradation due to the unmodeled disturbance torques. In the third simulation, we assume a simple disturbance torque model which only depends on the satellite's attitude quaternion (Case 3) to suggest a mitigation plan when the disturbance torques are partially predictable.

A. Case 1: Zero Disturbance Torque

In this case, the nominal process noise for the disturbance torque is set to be small as $q_d = (2.0 \cdot 10^{-7} \text{ Nm}/\sqrt{\text{hr}})^2$ in order to just prevent the filter from closing. Fig. 4 shows the estimation errors (solid line) and the $\pm 3\sigma$ bounds (dashed lines) estimated from the covariance matrix of the APKF. Note that most of the errors are within $\pm 3\sigma$ bounds, which represents that the APKF is working as expected.

The final 1σ is $(9.81, 8.01, 19.70)$ arcsec for attitude and $(49.08, 11.72, 15.89)$ arcsec/sec for body rate. The relative differences between the 1σ 's on each axis are qualitatively to be expected from the asymmetric body MOI, the asymmetric star tracker's accuracy, and the RW read-out noise. The 1σ is $(0.078, 0.079) \times 10^{-3} \text{ kgm}^2$ for (J_{yy}, J_{zz}) , which is less than 0.17 % of their nominal values, and 0.002 Am^2 for \vec{m} . The largest 1σ is 0.061 deg for $\vec{\delta}_{rw}$ and $0.61 \cdot 10^{-8} \text{ kgm}^2$ for \vec{J}_{rw} which is 0.2% of its nominal value. Note that the 1σ of $\vec{\omega}_{rw}$ remains almost same as R_{rw} , which implies that the RW speed read-out noise is the dominant noise that determines the filtering performance in the current system specification. In this case, it is worth considering removing $\vec{\omega}_{rw}$, $\vec{\omega}_{rw}^+$, and $\vec{\omega}_{rw}^-$ from the state vector to reduce state dimension and numerical burden.

B. Case 2: Sinusoidal Disturbance Torque

The most dominant unmodeled disturbance torque is the aerodynamic torque in low-earth orbit (LEO) [25]. The aerodynamic torque depends on the satellite's shape, attitude, altitude, and velocity. If we assume no other information on the aerodynamic torque other than its maximum magnitude, one approach is to set q_d large enough to prevent the 3σ of $\vec{\tau}_d$ from 3σ converging below the maximum disturbance. There are several studies about the order of magnitude of aerodynamic torques of a CubeSat in LEO: Gerhardt and Palo reported $8 \cdot 10^{-8} \text{ Nm}$ for a 3U CubeSat at

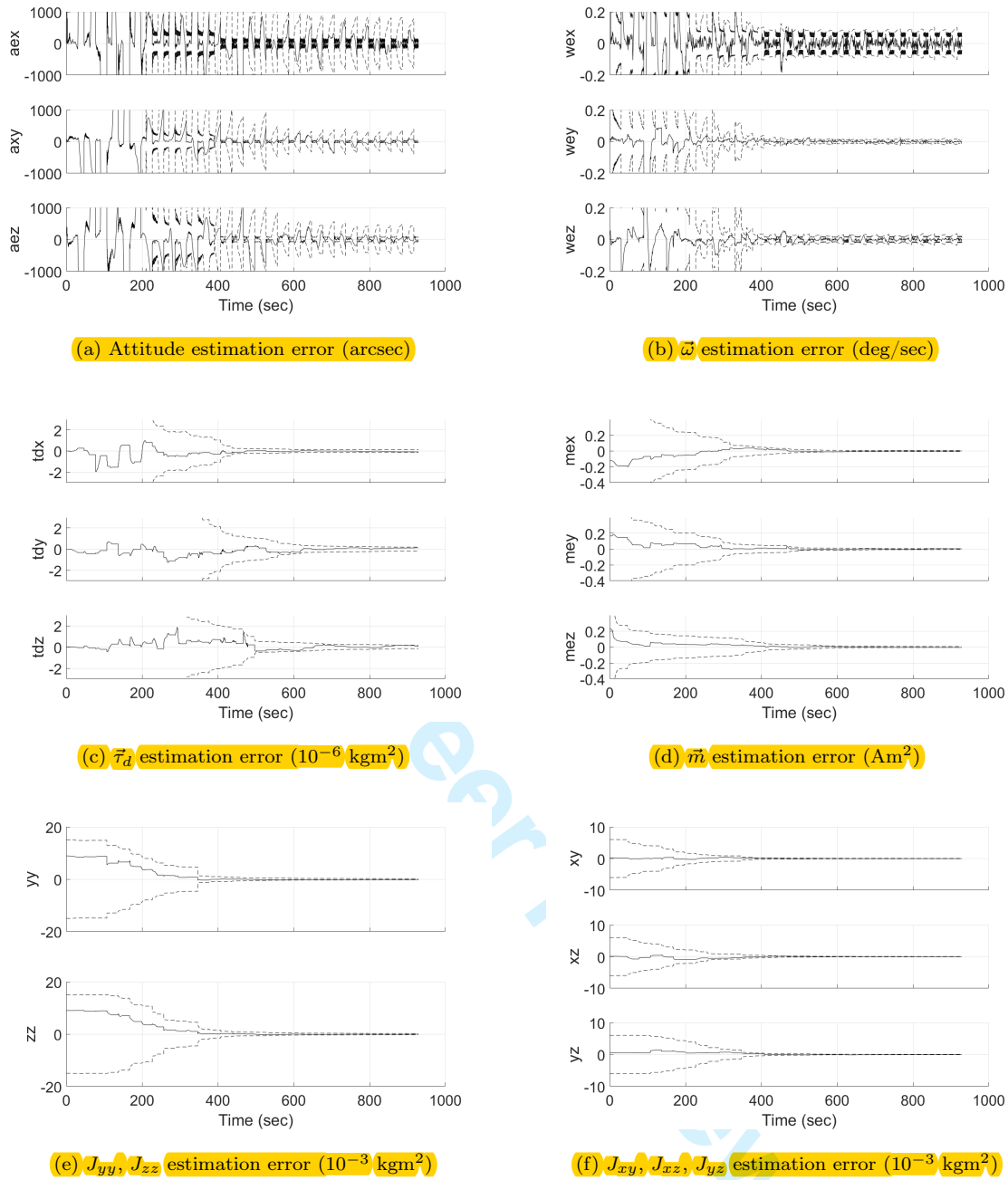


Fig. 4: Case 1 simulation results

600 km altitude [30], Rawashdeh and Lumpp reported $6 \cdot 10^{-7} \text{ Nm}$ for a 3U CubeSat at 400 km altitude [31], and Franquiz *et al.* reported $1 \cdot 10^{-6} \text{ Nm}$ for a 6U CubeSat at 500 km altitude [32].

To be conservative, we run the simulation with a nonharmonic sinusoidal disturbance torque model

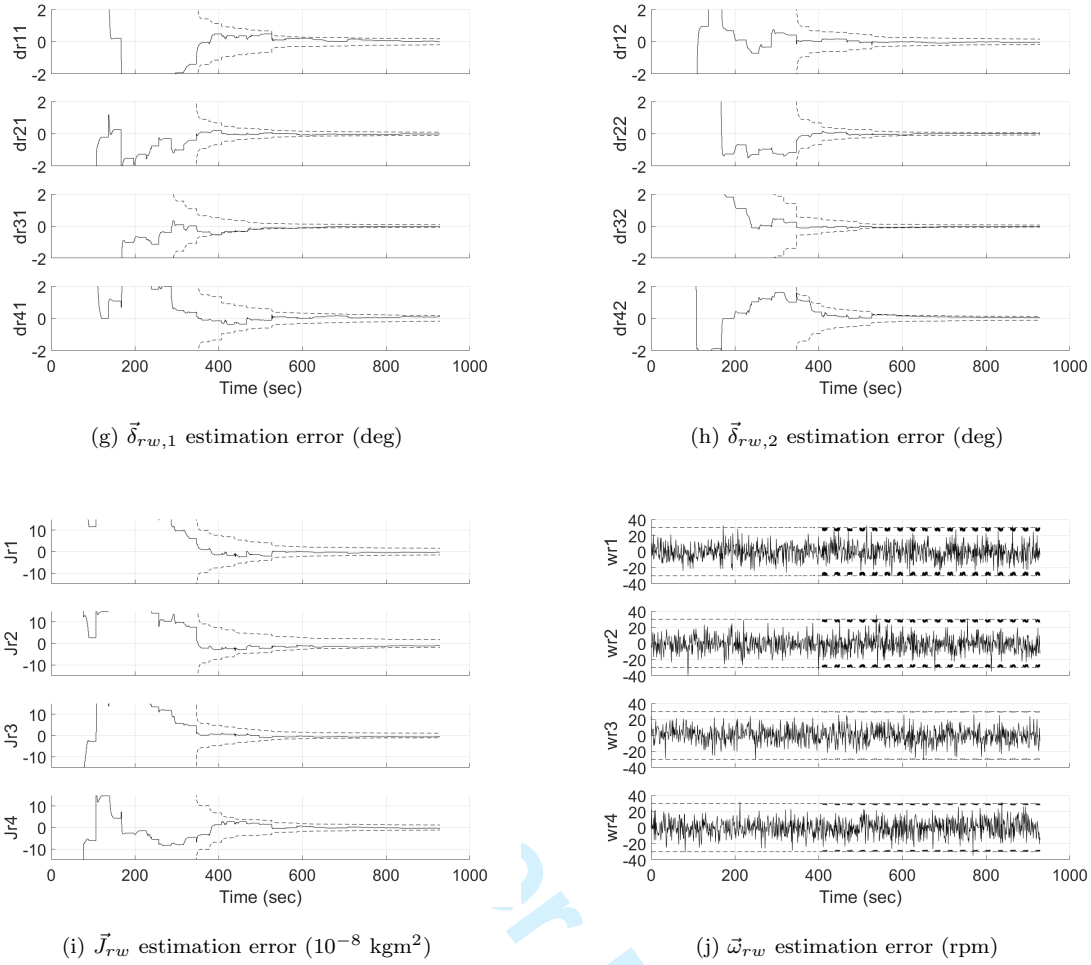


Fig. 4: Case 1 simulation results (continued)

whose magnitude is $\tau_{mag} = 1 \cdot 10^{-6}$ Nm as:

$$\vec{\tau}_d(t) = \tau_{mag} \begin{bmatrix} \sin(\frac{2\pi}{T_x}t + \theta_x) \\ \sin(\frac{2\pi}{T_y}t + \theta_y) \\ \sin(\frac{2\pi}{T_z}t + \theta_z) \end{bmatrix} \quad (115)$$

where t is time, $(T_x, T_y, T_z) = (80, 72.7, 82.47)$ sec, and $(\theta_x, \theta_y, \theta_z) = (90, 0, 135)$ deg. Note that this disturbance model does not represent the actual aerodynamic torque which is a function of the altitude, the velocity, and the attitude. Eq. (115) is just used to show the behavior of the APKF to the varying disturbance torques whose maximum magnitude is $1 \cdot 10^{-6}$ Nm. The covariance of the process noise is set to $q_d = (4.0 \cdot 10^{-6} \text{ Nm}/\sqrt{\text{hr}})^2$, which is 20 times greater than Case 1, to prevent the estimated covariance from becoming too small. This approach will degrade the performance of

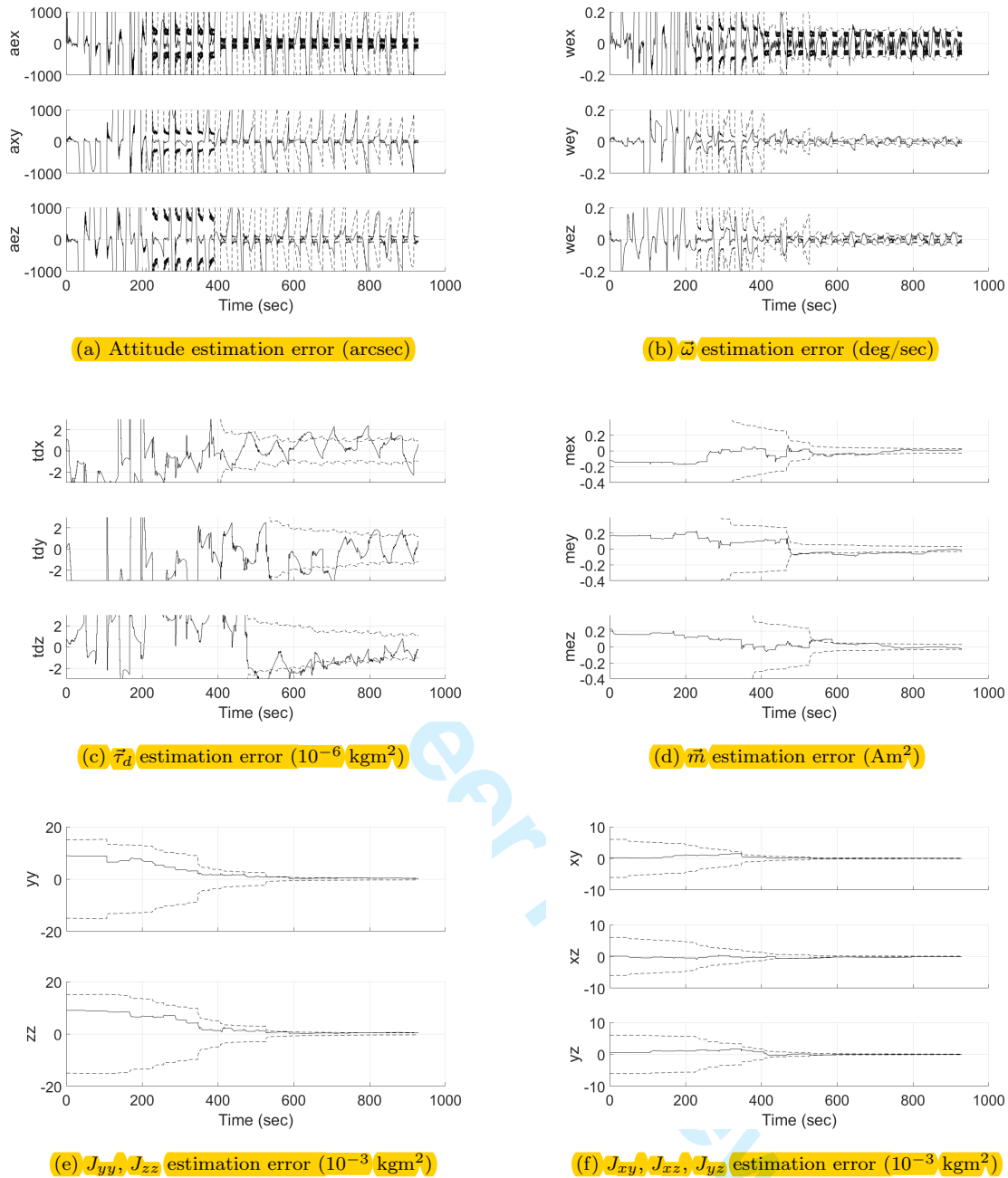


Fig. 5: Case 2 simulation results

the filter in terms of minimum covariance, but will help to keep the filter stable.

Fig. 5 shows the estimation errors and the $\pm 3\sigma$ bounds for Case 2. As intended, the $\vec{\tau}_d$ estimation errors are mostly kept inside of the $\pm 3\sigma$ bounds as Fig. 5 (c), so does the other state errors. The final 1σ is (9.83, 8.32, 21.19) arcsec for attitude and (49.33, 12.19, 17.13) arcsec/sec for body rate. The 1σ is (0.109, 0.123) $\times 10^{-3}$ kgm² for (J_{yy}, J_{zz}), and 0.011 Am² for \vec{m} . The largest 1σ is 0.13

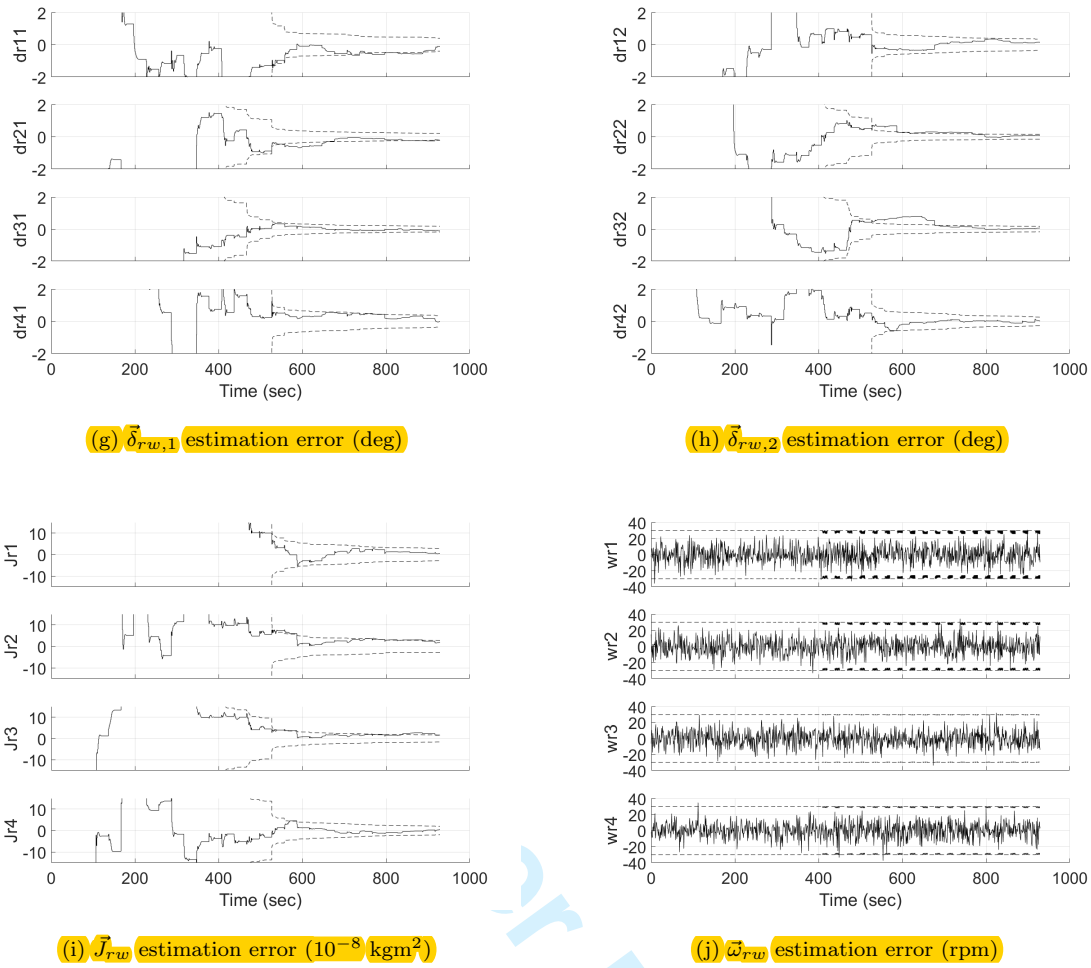


Fig. 5: Case 2 simulation results (continued)

deg for $\vec{\delta}_{rw}$ and $0.93 \cdot 10^{-8}$ kgm² for \vec{J}_{rw} . Compared to Case 1, the 1σ of attitude and body rate estimation is not much worse, but the 1σ for the other parameter estimates are 2 to 10 times bigger than Case 1's result. The effect of the degraded attitude parameter estimation is distinctly shown in the attitude and the rate estimation when the star tracker is not available for filter update. Comparing Fig. 5 (a) and (b) to Fig. 4 (a) and (b), the 3σ bounds of Case 2 increase much faster than Case 1 during the attitude maneuver. However, the APKF is still stable enough with this approach to deal with the unmodeled disturbance torque.

C. Case 3: Partially Predictable Disturbance Torque

Though the aerodynamic torque is also a function of the altitude and the velocity, the attitude in local vertical, local horizontal (LVLH) frame is the dominant factor that determines the disturbance torque in near-circular LEO. This means the variation of the aerodynamic torque depends on the body rates in the LVLH frame. Though it is difficult to represent this with an exact mathematical model, it is possible to adjust q_d to mitigate the filter performance degradation caused by large q_d in Case 2. In Case 3, a disturbance torque model given by Eq. (116) is used to simulate this property of the aerodynamic torque, and Fig. 6 shows the profile of the τ_d in Case 3.

$$\vec{\tau}_d = \tau_{mag} \begin{bmatrix} 1 - q_1 \\ 1 - q_2 \\ 1 - q_3 \end{bmatrix} \quad (116)$$

where $\tau_{mag} = 1 \cdot 10^{-6}$ Nm.

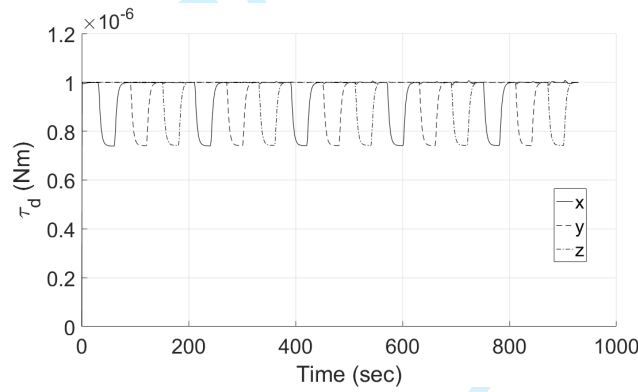


Fig. 6: Simplified disturbance torque model for Case 3

On the APKF side, $q_d = \text{diag}(q_{d,x}, q_{d,y}, q_{d,z})$ is tuned as follows:

$$q_{d,i} = q_{d0} + q_{d1} \cdot \hat{\omega}_i + q_{d2} \cdot |\hat{\vec{\omega}}| \quad (117)$$

where $i = x, y, z$. q_{d0} is for preventing the filter from closing as in Case 1, q_{d1} is for the linear variation of τ_d , and q_{d2} is for the variation coupled with the rotation in other directions, which is not included in Eq. (116). $q_{d0} = (2.0 \cdot 10^{-7} \text{ Nm}/\sqrt{\text{hr}})^2$, $q_{d1} = (2.0 \cdot 10^{-5} \text{ Nm}/\sqrt{\text{rad}})^2$, and $q_{d2} = 0.1 \cdot q_{d1}$ are used in this simulation.

Fig. 7 shows the estimation errors and the $\pm 3\sigma$ bounds for Case 3. The final 1σ is (9.82, 8.10,

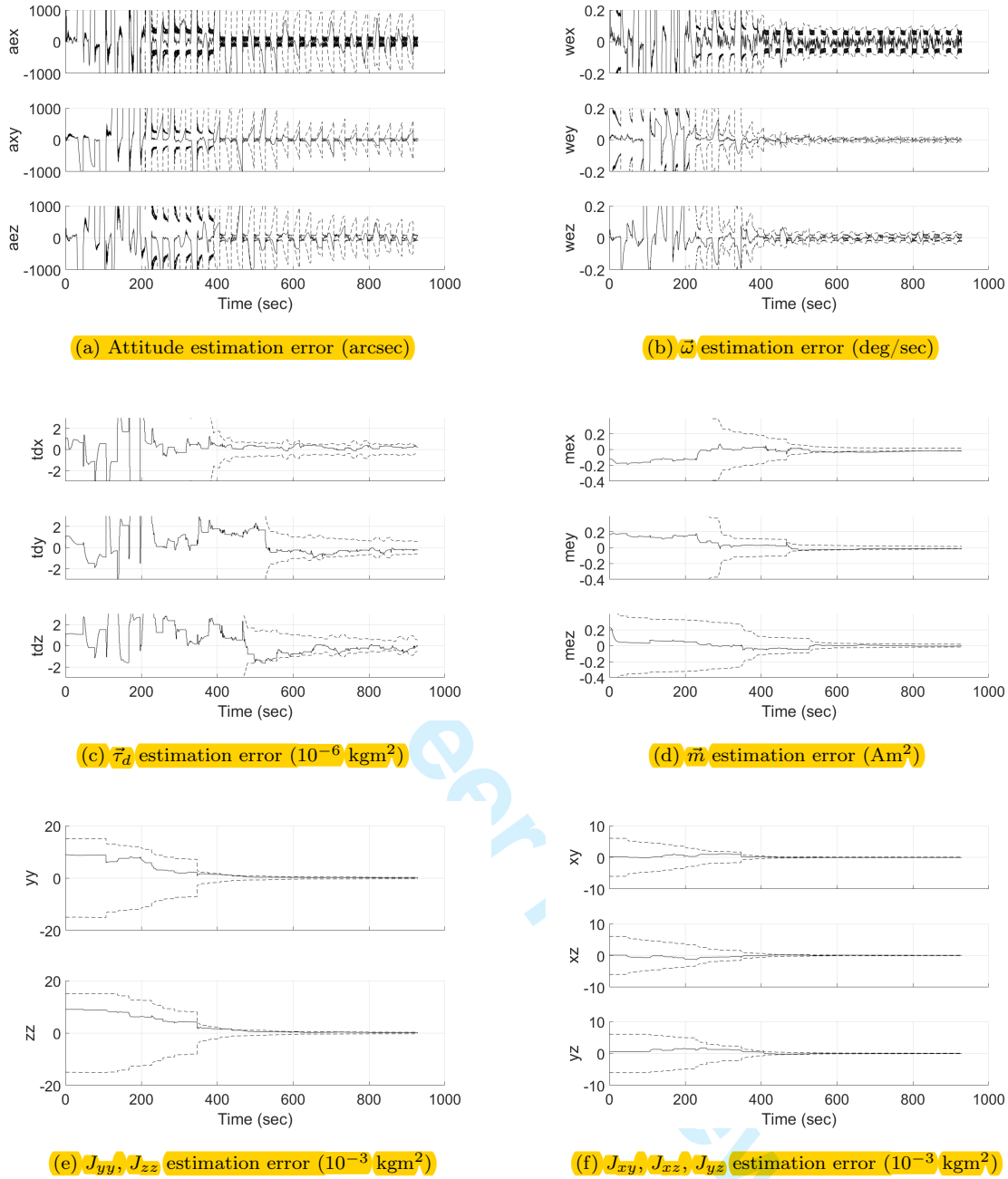


Fig. 7: Case 3 simulation results

20.88) arcsec for attitude and (49.37, 11.76, 17.01) arcsec/sec for body rate. The 1σ is (0.091, 0.095) $\times 10^{-3}$ kgm² for (J_{yy}, J_{zz}) , and 0.0056 Am² for \vec{m} . The largest 1σ is 0.072 deg for δ_{rw} and $0.71 \cdot 10^{-8}$ kgm² for \vec{J}_{rw} . Compared to Case 1, the 1σ for the attitude parameter estimates are 20% to 40% bigger than Case 1's result except \vec{m} . Note that this result is just for a hypothetical disturbance torque model given by Eq. (116), not for the actual aerodynamic torques, so we cannot

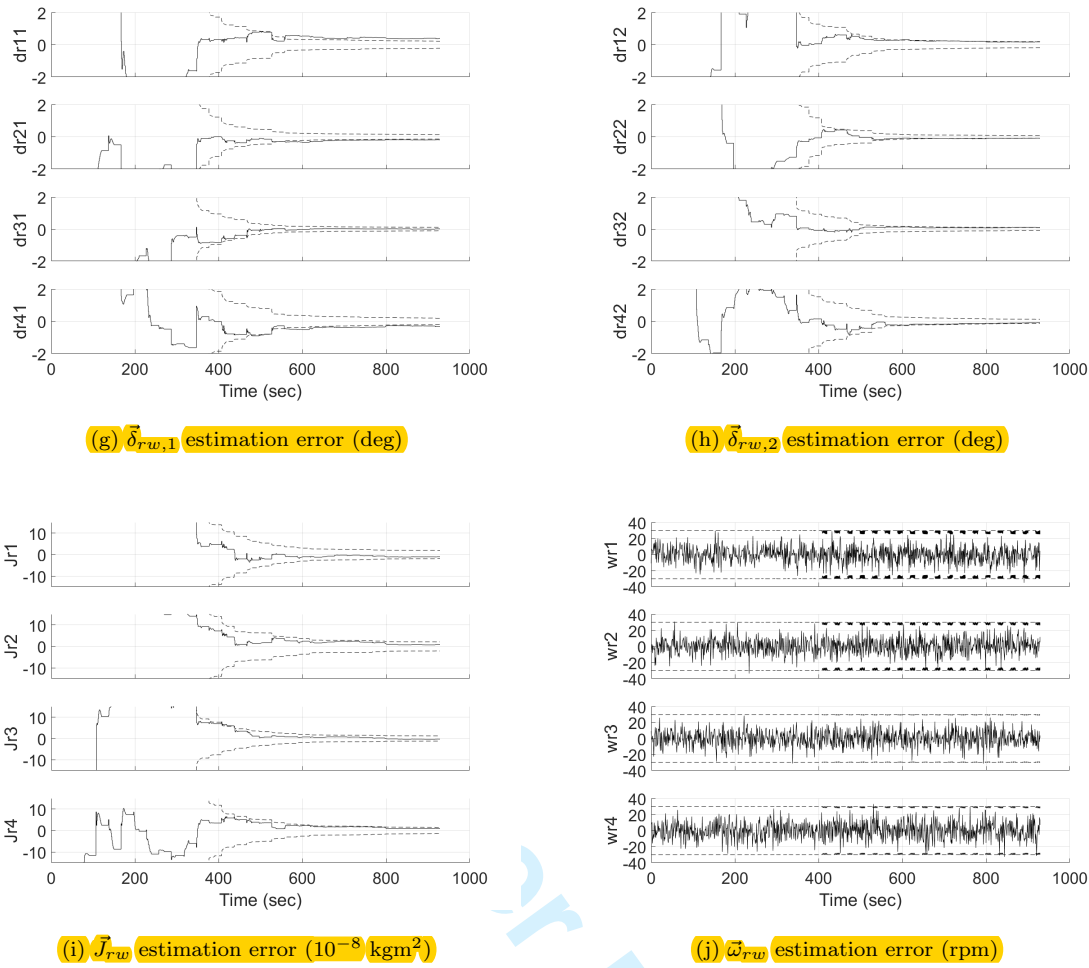


Fig. 7: Case 3 simulation results (continued)

guarantee the APKF's performance in a real system. However, this result shows that it is possible to mitigate the effect of the unmodeled disturbance torque by tuning the process noise covariance q_d even if we only have a partial and qualitative knowledge of it.

VIII. Conclusions

An attitude parameter calibration Kalman filter (APKF) that estimates attitude and body rate as well as the attitude parameters, which include spacecraft body moment of inertia (MOI), residual dipole moments, reaction wheel (RW) misalignments, and RW MOIs, was derived for gyro-less nanosatellites. Unlike the traditional onboard 6-state attitude determination Kalman filter, the APKF does not use gyroscope measurements in its system dynamics and uses the rigid-body dy-

namics to propagate its states. The partial-differential equation for error body rate was linearized with respect to the attitude parameters, and the state transition matrix was derived in a closed form for ease of implementation. To improve the filter's convergence, several physical and numerical approaches involving tuning the process noise covariance were proposed and the stability and performance of the APKF were demonstrated by simulations. We introduced two approaches to manage unmodeled disturbance torques, and demonstrated their utility in mitigating the effect of the unmodeled disturbance torques in simulation. These results are particularly useful for nanosatellite applications in which high accuracy gyroscopes are unavailable due to volume constraints. By incorporating rigid body dynamics into the Kalman filter, precision attitude determination can be achieved with only attitude sensors.

APPENDIX A: DERIVATION OF ERROR RATE DIFFERENTIAL EQUATION

This section describes the derivation of (51). With Eq. (43) and Eq. (48), the derivative of the error angular rate is written as:

$$\begin{aligned}
 \delta \dot{\vec{\omega}} &= \dot{\vec{\omega}} - \dot{\hat{\vec{\omega}}} \\
 &= (I - \hat{J}^{-1} \delta J) \hat{J}^{-1} [-(\hat{\vec{\omega}} + \delta \vec{\omega}) \times \{(\hat{J} + \delta J)(\hat{\vec{\omega}} + \delta \vec{\omega}) \\
 &\quad + (\hat{C}_{rw} + \delta C_{rw})(\hat{J}_{rw} + \delta J_{rw})(\hat{\vec{\omega}}_{rw} + \delta \vec{\omega}_{rw})\} \\
 &\quad - \frac{1}{\Delta t} (\hat{C}_{rw} + \delta C_{rw})(\hat{J}_{rw} + \delta J_{rw})(\hat{\vec{\omega}}_{rw}^+ + \delta \vec{\omega}_{rw}^+) - (\hat{\vec{\omega}}_{rw}^- + \delta \vec{\omega}_{rw}^-)) \\
 &\quad + \Psi(\vec{G}_b)(\hat{\vec{J}} + \delta \vec{J}) + (\hat{\vec{m}} + \delta \vec{m}) \times A(\hat{\vec{q}}) \vec{b}_i + \hat{\vec{\tau}}_d + \delta \vec{\tau}_d] \\
 &\quad - \hat{J}^{-1} [-\hat{\vec{\omega}} \times (\hat{J} \hat{\vec{\omega}} + \hat{C}_{rw} \hat{J}_{rw} \hat{\vec{\omega}}_{rw}) - \frac{1}{\Delta t} \hat{C}_{rw} \hat{J}_{rw} (\hat{\vec{\omega}}_{rw}^+ - \hat{\vec{\omega}}_{rw}^-) \\
 &\quad + \Psi(\vec{G}_b) \hat{\vec{J}} + \hat{\vec{m}} \times A(\hat{\vec{q}}) \vec{b}_i + \hat{\vec{\tau}}_d]
 \end{aligned} \tag{A1}$$

Regarding the gravity-gradient torque term, consider the following:

$$\begin{aligned}
 A(\hat{\vec{q}}) &= A(\delta \vec{q} \otimes \hat{\vec{q}}) = A(\delta \vec{q}) A(\hat{\vec{q}}) \\
 &\simeq (I - 2[\delta \vec{q} \times]) A(\hat{\vec{q}}) \\
 G_b &= A(\delta \vec{q} \otimes \hat{\vec{q}}) G_i A(\delta \vec{q} \otimes \hat{\vec{q}})^T \\
 &= A(\delta \vec{q}) A(\hat{\vec{q}}) G_i A(\hat{\vec{q}})^T A(\delta \vec{q})^T
 \end{aligned} \tag{A2}$$

$$\begin{aligned}
&\simeq (I - 2[\delta\vec{q}\times])\hat{G}_b(I + 2[\delta\vec{q}\times]) \\
&= \hat{G}_b - 2[\delta\vec{q}\times]\hat{G}_b + 2\hat{G}_b[\delta\vec{q}\times] - 4[\delta\vec{q}\times]\hat{G}_b[\delta\vec{q}\times]
\end{aligned} \tag{A3}$$

By ignoring the second order term $[\delta\vec{q}\times]\hat{G}_b[\delta\vec{q}\times]$, G_b can be expressed in a vector form of $\vec{G}_b = [G_{b11}, G_{b22}, G_{b33}, G_{b12}, G_{b13}, G_{b23}]^T$ as:

$$\begin{aligned}
\vec{G}_b &= \hat{G}_b - 2 \begin{bmatrix} 0 & 2\hat{G}_{b13} & -2\hat{G}_{b12} \\ -2\hat{G}_{b23} & 0 & 2\hat{G}_{b12} \\ 2\hat{G}_{b23} & -2\hat{G}_{b13} & 0 \\ -\hat{G}_{b13} & \hat{G}_{b23} & (\hat{G}_{b11} - \hat{G}_{b22}) \\ \hat{G}_{b12} & (\hat{G}_{b33} - \hat{G}_{b11}) & -\hat{G}_{b23} \\ (\hat{G}_{b22} - \hat{G}_{b33}) & -\hat{G}_{b12} & \hat{G}_{b13} \end{bmatrix} \delta\vec{q} \\
&= \hat{G}_b - 2\Upsilon(\hat{G}_b)\delta\vec{q}
\end{aligned} \tag{A4}$$

By expanding and ignoring the second or higher order terms with Eq. (A2) and Eq. (A4), (A1) becomes

$$\begin{aligned}
\delta\dot{\vec{\omega}} &= \hat{J}^{-1}[-\hat{\vec{\omega}} \times (\delta J \hat{\vec{\omega}} + \hat{J} \delta \vec{\omega} + \delta C_{rw} \hat{J}_{rw} \hat{\vec{\omega}}_{rw} + \hat{C}_{rw} \delta J_{rw} \hat{\vec{\omega}}_{rw} + \hat{C}_{rw} \hat{J}_{rw} \delta \vec{\omega}_{rw}) \\
&\quad + \delta C_{rw} \hat{\vec{t}}_{rw} - \hat{C}_{rw} \delta J_{rw} \hat{\vec{\alpha}}_{rw} - \frac{1}{\Delta t} \hat{C}_{rw} \hat{J}_{rw} (\delta \vec{\omega}_{rw}^+ - \delta \vec{\omega}_{rw}^-) \\
&\quad - \delta \vec{\omega} \times \hat{H}_t + \Psi(\hat{G}_b) \delta \vec{J} + 2\Psi(\hat{J}) \Upsilon(\hat{G}_b) \delta \vec{q} \\
&\quad + \delta \vec{m} \times \hat{\vec{b}}_b - \hat{\vec{m}} \times (2[\delta\vec{q}\times]\hat{\vec{b}}_b) + \delta \vec{\tau}_d - \delta J \hat{J}^{-1} \hat{\vec{\tau}}_t]
\end{aligned} \tag{A5}$$

where

$$\hat{\vec{h}}_{rw} = \hat{J}_{rw} \hat{\vec{\omega}}_{rw} \tag{A6}$$

$$\hat{\vec{\alpha}}_{rw} = \frac{1}{\Delta t} (\hat{\vec{\omega}}_{rw}^+ - \hat{\vec{\omega}}_{rw}^-) \tag{A7}$$

$$\hat{\vec{t}}_{rw} = -\hat{J}_{rw} \hat{\vec{\alpha}}_{rw} \tag{A8}$$

$$\hat{H}_t = \hat{J} \hat{\vec{\omega}} + \hat{C}_{rw} \hat{\vec{h}}_{rw} \tag{A9}$$

$$\hat{\vec{\tau}}_t = -\hat{\vec{\omega}} \times \hat{H}_t + \hat{C}_{rw} \hat{\vec{t}}_{rw} + \Psi(\hat{G}_b) \hat{\vec{J}} + \hat{\vec{m}} \times \hat{\vec{b}}_b + \hat{\vec{\tau}}_d \tag{A10}$$

$$D(\vec{v}) = \text{diag}(\vec{v}) \tag{A11}$$

$$\hat{C}_{rw} = C_{rw,0} + C_{rw,1} D(\hat{\vec{\omega}}_{rw,1}) + C_{rw,2} D(\hat{\vec{\omega}}_{rw,2}) \tag{A12}$$

and

$$\begin{aligned}\delta C_{rw} &= C_{rw} - \hat{C}_{rw} \\ &= C_{rw,1}D(\Delta\vec{\delta}_{rw,1}) + C_{rw,2}D(\Delta\vec{\delta}_{rw,2})\end{aligned}\quad (A13)$$

Note that $\delta\vec{\omega}_{rw}$ and $\delta\vec{\omega}_{rw}^-$ are not the same. $\delta\vec{\omega}_{rw}^-$ is $\delta\vec{\omega}_{rw}$ at the measurement time of $\delta\vec{\omega}_{rw}^-$, and it remains constant. $\delta\vec{\omega}_{rw}$ represents the uncertainty of the RW speed through time, so its uncertainty changes through time. In order to apply the Kalman filter approach, (A5) should be expressed in $\dot{\vec{x}} = F\vec{x} + G\vec{\eta}$ form. Since (A5) contains so many terms, let us consider the terms related each error state one by one. Regarding $\delta\vec{q}$,

$$\begin{aligned}\delta\dot{\vec{\omega}}|_{\delta\vec{q}} &= \hat{J}^{-1}\{2\Psi(\hat{J})\Upsilon(\hat{G}_b)\delta\vec{q} - \hat{m} \times (2[\delta\vec{q} \times] \hat{b}_b)\} \\ &= \hat{J}^{-1}\{2\Psi(\hat{J})\Upsilon(\hat{G}_b)\delta\vec{q} + 2[\hat{m} \times][\hat{b}_b \times]\delta\vec{q}\} \\ &= 2\hat{J}^{-1}\{\Psi(\hat{J})\Upsilon(\hat{G}_b) + [\hat{m} \times][\hat{b}_b \times]\}\delta\vec{q}\end{aligned}\quad (A14)$$

Regarding $\delta\vec{\omega}$,

$$\begin{aligned}\delta\dot{\vec{\omega}}|_{\delta\vec{\omega}} &= \hat{J}^{-1}\{-\hat{\omega} \times \hat{J}\delta\vec{\omega} - \delta\vec{\omega} \times \hat{H}_t\} \\ &= \hat{J}^{-1}\{-\hat{\omega} \times \hat{J}\delta\vec{\omega} + \hat{H}_t \times \delta\vec{\omega}\} \\ &= \hat{J}^{-1}\{-[\hat{\omega} \times]\hat{J} + [\hat{H}_t \times]\}\delta\vec{\omega}\end{aligned}\quad (A15)$$

Regarding $\delta\vec{\tau}_d$,

$$\delta\dot{\vec{\omega}}|_{\delta\vec{\tau}_d} = \hat{J}^{-1}\delta\vec{\tau}_d \quad (A16)$$

Regarding $\delta\vec{J}$,

$$\delta\dot{\vec{\omega}}|_{\delta\vec{J}} = \hat{J}^{-1}\{-\hat{\omega} \times \delta J\hat{\omega} + \Psi(\hat{G}_b)\delta\vec{J} - \delta J\hat{J}^{-1}\hat{\tau}_t\} \quad (A17)$$

Since δJ is a symmetric 3 by 3 matrix as:

$$\delta J = \begin{bmatrix} \delta J_{xx} & \delta J_{xy} & \delta J_{xz} \\ \delta J_{xy} & \delta J_{yy} & \delta J_{yz} \\ \delta J_{xz} & \delta J_{yz} & \delta J_{zz} \end{bmatrix} \quad (A18)$$

and $\delta\vec{J}$ is a 6 by 1 vector as:

$$\delta\vec{J} = \begin{bmatrix} \delta J_{xx} & \delta J_{yy} & \delta J_{zz} & \delta J_{xy} & \delta J_{xz} & \delta J_{yz} \end{bmatrix}^T \quad (\text{A19})$$

the following identity holds for any 3 by 1 vector $\vec{v} = [v_1, v_2, v_3]^T$.

$$\delta J \vec{v} = \Omega(\vec{v}) \delta\vec{J} \quad (\text{A20})$$

where

$$\Omega(\vec{v}) = \begin{bmatrix} v_1 & 0 & 0 & v_2 & v_3 & 0 \\ 0 & v_2 & 0 & v_1 & 0 & v_3 \\ 0 & 0 & v_3 & 0 & v_1 & v_2 \end{bmatrix} \quad (\text{A21})$$

Therefore, (A17) can be written as:

$$\delta\dot{\vec{\omega}}|_{\delta\vec{J}} = \hat{J}^{-1} \{ \Psi(\hat{G}_b) - [\hat{\omega} \times] \Omega(\hat{\omega}) - \Omega(\hat{J}^{-1} \hat{\tau}_t) \} \delta\vec{J} \quad (\text{A22})$$

Regarding $\delta\vec{m}$,

$$\delta\dot{\vec{\omega}}|_{\delta\vec{m}} = \hat{J}^{-1} (\delta\vec{m} \times \hat{b}_b) = -\hat{J}^{-1} [\hat{b}_b \times] \delta\vec{m} \quad (\text{A23})$$

Regarding δC_{rw} or $\Delta\vec{\delta}_{rw}$,

$$\delta\dot{\vec{\omega}}|_{\delta C_{rw}} = \hat{J}^{-1} \{ -[\hat{\omega} \times] \delta C_{rw} \hat{h}_{rw} - \delta C_{rw} \hat{t}_{rw} \} \quad (\text{A24})$$

In order to make (A24) in vector form, let us consider the following identity for any n by 1 vector \vec{v} .

$$\begin{aligned} \delta C_{rw} \vec{v} &= C_{rw,1} D(\Delta\vec{\delta}_{rw,1}) \vec{v} + C_{rw,2} D(\Delta\vec{\delta}_{rw,2}) \vec{v} \\ &= C_{rw,1} D(\vec{v}) \Delta\vec{\delta}_{rw,1} + C_{rw,2} D(\vec{v}) \Delta\vec{\delta}_{rw,2} \\ &= \begin{bmatrix} \vec{c}_{1,1} v_1 & \cdots & \vec{c}_{n,1} v_n \end{bmatrix} \Delta\vec{\delta}_{rw,1} + \begin{bmatrix} \vec{c}_{1,2} v_1 & \cdots & \vec{c}_{n,2} v_n \end{bmatrix} \Delta\vec{\delta}_{rw,2} \\ &= \begin{bmatrix} \vec{c}_{1,1} v_1 & \cdots & \vec{c}_{n,1} v_n & \vec{c}_{1,2} v_1 & \cdots & \vec{c}_{n,2} v_n \end{bmatrix} \begin{bmatrix} \Delta\vec{\delta}_{rw,1} \\ \Delta\vec{\delta}_{rw,2} \end{bmatrix} \\ &= C(\vec{v}) \Delta\vec{\delta}_{rw} \end{aligned} \quad (\text{A25})$$

where $C(\vec{v})$ is defined as:

$$C(\vec{v}) = \begin{bmatrix} \vec{c}_{1,1} v_1 & \vec{c}_{2,1} v_2 & \cdots & \vec{c}_{n,1} v_n & \vec{c}_{1,2} v_1 & \vec{c}_{2,2} v_2 & \cdots & \vec{c}_{n,2} v_n \end{bmatrix} \quad (\text{A26})$$

Using (A25), (A24) becomes

$$\delta\dot{\vec{\omega}}|_{\delta C_{rw}} = \hat{J}^{-1}\{-[\hat{\vec{\omega}}\times]C(\hat{h}_{rw}) + C(\hat{t}_{rw})\}\Delta\vec{\delta}_{rw} \quad (\text{A27})$$

Regarding $\delta\vec{J}_{rw}$,

$$\delta\dot{\vec{\omega}}|_{\delta\vec{J}_{rw}} = \hat{J}^{-1}\{-[\hat{\vec{\omega}}\times]\hat{C}_{rw}\delta J_{rw}\hat{\vec{\omega}}_{rw} - \hat{C}_{rw}\delta J_{rw}\hat{\vec{\alpha}}_{rw}\} \quad (\text{A28})$$

Since $\delta J_{rw} = D(\delta\vec{J}_{rw})$ and $D(\vec{a})\vec{b} = D(\vec{b})\vec{a}$, (A28) can be written as:

$$\delta\dot{\vec{\omega}}|_{\delta\vec{J}_{rw}} = \hat{J}^{-1}\{-[\hat{\vec{\omega}}\times]\hat{C}_{rw}D(\hat{\vec{\omega}}_{rw}) - \hat{C}_{rw}D(\hat{\vec{\alpha}}_{rw})\}\delta\vec{J}_{rw} \quad (\text{A29})$$

Regarding $\delta\vec{\omega}_{rw}$, $\delta\vec{\omega}_{rw}^-$, and $\delta\vec{\omega}_{rw}^+$,

$$\delta\dot{\vec{\omega}}|_{\delta\vec{\omega}_{rw}} = -\hat{J}^{-1}[\hat{\vec{\omega}}\times]\hat{C}_{rw}\hat{J}_{rw}\delta\vec{\omega}_{rw} \quad (\text{A30})$$

$$\delta\dot{\vec{\omega}}|_{\delta\vec{\omega}_{rw}^-} = \frac{1}{\Delta t}\hat{J}^{-1}\hat{C}_{rw}\hat{J}_{rw}\delta\vec{\omega}_{rw}^- \quad (\text{A31})$$

$$\delta\dot{\vec{\omega}}|_{\delta\vec{\omega}_{rw}^+} = -\frac{1}{\Delta t}\hat{J}^{-1}\hat{C}_{rw}\hat{J}_{rw}\delta\vec{\omega}_{rw}^+ \quad (\text{A32})$$

Combining (A14)-(A16), (A22), (A23), (A27), (A29), and (A30)-(A32),

$$\begin{aligned} \delta\dot{\vec{\omega}} = & 2\hat{J}^{-1}\{\Psi(\hat{J})\Upsilon(\hat{G}_b) + [\hat{m}\times][\hat{b}_b\times]\}\delta\vec{q} + \hat{J}^{-1}\{-[\hat{\vec{\omega}}\times]\hat{J} + [\hat{H}_t\times]\}\delta\vec{\omega} + \hat{J}^{-1}\delta\vec{\tau}_d \\ & + \hat{J}^{-1}\{\Psi(\hat{G}_b) - [\hat{\vec{\omega}}\times]\Omega(\hat{\vec{\omega}}) - \Omega(\hat{J}^{-1}\hat{\vec{\tau}}_t)\}\delta\vec{J} - \hat{J}^{-1}[\hat{b}_b\times]\delta\vec{m} \\ & + \hat{J}^{-1}\{-[\hat{\vec{\omega}}\times]C(\hat{h}_{rw}) + C(\hat{t}_{rw})\}\Delta\vec{\delta}_{rw} + \hat{J}^{-1}\{-[\hat{\vec{\omega}}\times]\hat{C}_{rw}D(\hat{\vec{\omega}}_{rw}) - \hat{C}_{rw}D(\hat{\vec{\alpha}}_{rw})\}\delta\vec{J}_{rw} \\ & - \hat{J}^{-1}[\hat{\vec{\omega}}\times]\hat{C}_{rw}\hat{J}_{rw}\delta\vec{\omega}_{rw} + \frac{1}{\Delta t}\hat{J}^{-1}\hat{C}_{rw}\hat{J}_{rw}\delta\vec{\omega}_{rw}^- - \frac{1}{\Delta t}\hat{J}^{-1}\hat{C}_{rw}\hat{J}_{rw}\delta\vec{\omega}_{rw}^+ \end{aligned} \quad (\text{A33})$$

APPENDIX B: DERIVATION OF STATE TRANSITION MATRIX

The state transition matrix Φ satisfies:

$$\dot{\Phi}(t) = F\Phi(t) \quad (\text{B1})$$

$$\Phi(0) = I \quad (\text{B2})$$

where F is given in Eq. (63). Let us consider Φ partitioned into block matrices as:

$$\Phi = \begin{bmatrix} \phi_{11} & \phi_{12} & \cdots & \phi_{1a} \\ \phi_{21} & \phi_{22} & \cdots & \phi_{2a} \\ \vdots & \vdots & \ddots & \vdots \\ \phi_{a1} & \phi_{a2} & \cdots & \phi_{aa} \end{bmatrix} \quad (\text{B3})$$

Eq. (B1) can be written as:

$$\begin{bmatrix} \dot{\phi}_{11} & \dot{\phi}_{12} & \cdots & \dot{\phi}_{1a} \\ \dot{\phi}_{21} & \dot{\phi}_{22} & \cdots & \dot{\phi}_{2a} \\ \vdots & \vdots & \ddots & \vdots \\ \dot{\phi}_{a1} & \dot{\phi}_{a2} & \cdots & \dot{\phi}_{aa} \end{bmatrix} = \begin{bmatrix} -[\hat{\omega} \times] & \frac{1}{2}I & 0 & \cdots & 0 \\ F_{21} & F_{22} & F_{23} & \cdots & F_{2a} \\ & & 0 & & \\ & & & \ddots & F_{89} & F_{8a} \\ & & & & 0 & \\ & & & & & 0 \end{bmatrix} \begin{bmatrix} \phi_{11} & \phi_{12} & \cdots & \phi_{1a} \\ \phi_{21} & \phi_{22} & \cdots & \phi_{2a} \\ \vdots & \vdots & \ddots & \vdots \\ \phi_{a1} & \phi_{a2} & \cdots & \phi_{aa} \end{bmatrix} \quad (\text{B4})$$

The j -th column of $\dot{\Phi}$ can be expanded as:

$$\dot{\phi}_{1j} = -[\hat{\omega} \times] \phi_{1j} + \frac{1}{2} \phi_{2j} \quad (\text{B5})$$

$$\dot{\phi}_{2j} = \sum_{k=1}^a F_{2k} \phi_{kj} \quad (\text{B6})$$

$$\dot{\phi}_{8j} = F_{89} \phi_{9j} + F_{8a} \phi_{aj} \quad (\text{B7})$$

$$\dot{\phi}_{lj} = 0 \quad (\text{B8})$$

with the boundary condition:

$$\phi_{ij}(0) = \begin{cases} I, & \text{if } i = j \\ 0, & \text{otherwise} \end{cases} \quad (\text{B9})$$

for $l = 3, \dots, 7, 9, a$.

For $j = 1$: It is obvious that $\phi_{i1} = 0$ from Eq. (B7) and Eq. (B8) for $i = 3, \dots, a$. Then, Eq. (B5) and Eq. (B6) becomes:

$$\dot{\phi}_{11} = -[\hat{\omega} \times] \phi_{11} + \frac{1}{2} \phi_{21} \quad (\text{B10})$$

$$\dot{\phi}_{21} = F_{21} \phi_{11} + F_{22} \phi_{21} \quad (\text{B11})$$

Since $\phi_{21}(0) = 0$ and $F_{21} \ll I$,

$$\begin{aligned} \dot{\phi}_{11} &\simeq -[\hat{\omega} \times] \phi_{11} \\ \phi_{11} &\simeq I - [\hat{\omega} \times] \Delta t \end{aligned} \quad (\text{B12})$$

Useful approximation: the definite integral solution of $\dot{\phi}(t) = A\phi(t) + B(t)$, where A is constant, $B(t)$ is a function of t , and $\phi(t_0) = 0$, is known as:

$$\begin{aligned}\phi(t_1) &= \frac{\int_{t_0}^{t_1} e^{\int -Adt'|_{\tau}} B(\tau) d\tau}{e^{\int -Adt'|_{t_1}}} \\ &= \int_{t_0}^{t_1} e^{\int_{\tau}^{t_1} Adt'} B(\tau) d\tau \\ &\simeq \int_{t_0}^{t_1} [I + A(t_1 - \tau)] B(\tau) d\tau\end{aligned}\quad (B13)$$

This approximation will be repeatedly used in the following derivations. From Eq. (B11), Eq. (B12), and Eq. (B13), ϕ_{21} is approximated as:

$$\phi_{21} = F_{21}\Delta t + \frac{1}{2}(F_{22}F_{21} - F_{21}[\hat{\omega} \times])\Delta t^2 - \frac{1}{6}F_{22}F_{21}[\hat{\omega} \times]\Delta t^3 \quad (B14)$$

For $j = 2$: Similar to above, it is possible to derive the following:

$$\phi_{12} = \frac{1}{2}(I\Delta t - \frac{1}{2}[\hat{\omega} \times]\Delta t^2 + \frac{1}{2}F_{22}\Delta t^2 - \frac{1}{6}[\hat{\omega} \times]F_{22}\Delta t^3) \quad (B15)$$

$$\phi_{22} = I + F_{22}\Delta t + \frac{1}{2}F_{22}^2\Delta t^2 \quad (B16)$$

$$\phi_{i2} = 0 \quad (B17)$$

for $i = 3, \dots, a$.

For $j = 3, \dots, 8$: From Eq. (B7), Eq. (B8), and Eq. (B9),

$$\phi_{ij}(t) = \begin{cases} I, & \text{if } i = j \\ 0, & \text{otherwise} \end{cases} \quad (B18)$$

for $i = 3, 4, \dots, a$. From Eq. (B5), Eq. (B6), Eq. (B18), and the fact that $F_{21} \ll I$ and $\phi_{1j}(0) = 0$,

$$\dot{\phi}_{1j} = -[\hat{\omega} \times]\phi_{1j} + \frac{1}{2}\phi_{2j} \quad (B19)$$

$$\begin{aligned}\dot{\phi}_{2j} &= F_{21}\phi_{1j} + F_{22}\phi_{2j} + F_{2j} \\ &\simeq F_{22}\phi_{2j} + F_{2j}\end{aligned}\quad (B20)$$

Applying Eq. (B13) to Eq. (B20),

$$\phi_{2j} \simeq F_{2j}\Delta t + \frac{1}{2}F_{22}F_{2j}\Delta t^2 \quad (B21)$$

With Eq. (B21), Eq. (B19) becomes

$$\dot{\phi}_{1j}(t) = -[\hat{\omega} \times] \phi_{1j} + \frac{1}{2} [F_{2j}(t - t_0) + \frac{1}{2} F_{22} F_{2j}(t - t_0)^2] \quad (\text{B22})$$

Applying Eq. (B13),

$$\phi_{1j} \simeq \frac{1}{4} F_{2j} \Delta t^2 - \frac{1}{12} [\hat{\omega} \times] F_{2j} \Delta t^3 + \frac{1}{12} F_{22} F_{2j} \Delta t^3 - \frac{1}{48} [\hat{\omega} \times] F_{22} F_{2j} \Delta t^4 \quad (\text{B23})$$

For $j = 9, a$: From Eq. (B7), Eq. (B8), and Eq. (B9),

$$\phi_{ij}(t) = \begin{cases} I, & \text{if } i = j \\ 0, & \text{otherwise} \end{cases} \quad (\text{B24})$$

for $i = 3, \dots, 7, 9, a$. Then, Eqs. (B5)- (B7) become

$$\dot{\phi}_{1j} = -[\hat{\omega} \times] \phi_{1j} + \frac{1}{2} \phi_{2j} \quad (\text{B25})$$

$$\dot{\phi}_{2j} \simeq F_{22} \phi_{2j} + F_{28} \phi_{8j} + F_{2j} \quad (\text{B26})$$

$$\dot{\phi}_{8j} = F_{8j} \quad (\text{B27})$$

Since $\phi_{8j}(0) = 0$,

$$\phi_{8j} = F_{8j} \Delta t \quad (\text{B28})$$

So,

$$\dot{\phi}_{2j} = F_{22} \phi_{2j} + F_{28} F_{8j} \Delta t + F_{2j} \quad (\text{B29})$$

$$\phi_{2j} \simeq F_{2j} \Delta t + \frac{1}{2} F_{22} F_{2j} \Delta t^2 + \frac{1}{2} F_{28} F_{8j} \Delta t^2 + \frac{1}{6} F_{22} F_{28} F_{8j} \Delta t^3 \quad (\text{B30})$$

and

$$\begin{aligned} \dot{\phi}_{1j} &= -[\hat{\omega} \times] \phi_{1j} + \frac{1}{2} [F_{2j} \Delta t + \frac{1}{2} F_{22} F_{2j} \Delta t^2 + \frac{1}{2} F_{28} F_{8j} \Delta t^2 + \frac{1}{6} F_{22} F_{28} F_{8j} \Delta t^3] \\ \phi_{1j} &= \frac{1}{4} F_{2j} \Delta t^2 + \frac{1}{12} (F_{22} F_{2j} + F_{28} F_{8j} - [\hat{\omega} \times] F_{2j}) \Delta t^3 \\ &\quad + \frac{1}{48} [F_{22} F_{28} F_{8j} - [\hat{\omega} \times] (F_{22} F_{2j} + F_{28} F_{8j})] \Delta t^4 - \frac{1}{240} [\hat{\omega} \times] F_{22} F_{28} F_{8j} \Delta t^5 \end{aligned} \quad (\text{B31})$$

ACKNOWLEDGMENTS

Hyosang Yoon acknowledges support from Samsung Scholarship.

REFERENCES

- [1] Lefferts, E. E., Markley, F. L., and Shuster, M. D., "Kalman Filtering for Spacecraft Attitude Estimation," *Journal of Guidance, Control, and Dynamics*, Vol. 5, No. 5, 1982, pp. 417-429. doi:10.2514/3.56190
- [2] Mehrparvar, A., "Cubesat Design Specification Rev. 13," *Cal Poly*, California Polytechnic State Univ., San Luis Obispo, CA, February. 2014, http://www.cubesat.org/s/cds_rev13_final2.pdf, [retrieved December 1, 2016].
- [3] Hand, E., "Startup liftoff," *Science*, Vol. 348, No. 6231, 2015, pp. 172-177. doi:10.1126/science.348.6231.172
- [4] Knapp, A., "Spire to Launch Constellation Of Cubesats For Weather Forecasting," *Forbes*, 2015, <http://www.forbes.com/sites/alexknapp/2015/01/29/spire-to-launch-constellation-of-cubesats-for-weather-forecasting/#7bd3c5dade9a> [retrieved February 1 2017].
- [5] *Guide to Comparing Gyro and IMU Technologies - Micro-Electro-Mechanical Systems and Fiber Optic Gyros*, KVH Industries, Inc. Report, Middletown, Rhode Island, 2014.
- [6] Rawashdeh, S. A., Lumpp, J. E. J., Barrington-Brown, J., and Pastena, M., "A Stellar Gyroscope for Small Satellite Attitude Determination," *Proceedings of the AIAA/USU Conference on Small Satellites*, Advanced Technologies II, SSC12-IX-7, 2012.
- [7] Johnston-Lemke, B., Sarda, K., Grant, C. C., and Zee, R. E., "Arc-Minute Attitude Stability on a Nanosatellite: Enabling Stellar Photometry on the Smallest Scale," *Proceedings of the AIAA/USU Conference on Small Satellites*, Mission Enabling Technologies II, SSC11-X-7, 2011.
- [8] Sarda, K., Grant, C. C., Chaumont, M., Choi, S. Y., Johnston-Lemke, B., and Zee, R. E., "On-Orbit Performance of the Bright Target Explorer (BRITE) Nanosatellite Astronomy Constellation," *Proceedings of the AIAA/USU Conference on Small Satellites*, Year in Review, SSC14-XII-6, 2014.
- [9] Shuster, M. D., Pitone, D. S., and Bierman, G. J., "Batch Estimation of Spacecraft Sensor Alignments I. Relative Alignment Estimation," *Journal of Astronautical Sciences*, Vol. 39, No. 4, 1991, pp. 519-546.
- [10] Shuster, M. D. and Pitone, D. S., "Batch Estimation of Spacecraft Sensor Alignments II. Absolute Alignment Estimation," *Journal of Astronautical Sciences*, Vol. 39, No. 4, 1991, pp. 547-571.
- [11] Pittelkau, M. E., "Kalman Filtering for Spacecraft System Alignment Calibration," *Journal of Guidance, Control, and Dynamics*, Vol. 24, No. 6, 2001, pp. 1187-1195. doi:10.2514/2.4834
- [12] Pittelkau, M. E., "Everything Is Relative in Spacecraft System Alignment Calibration," *Journal of Spacecraft and Rockets*, Vol. 39, No. 3, 2002, pp. 460-466. doi:10.2514/2.3830

- [13] Zanardi, M. C. and Shuster, M. D., "Batch, Sequential and Hybrid Approaches to Spacecraft Sensor Alignment Estimation," *Journal of Astronautical Sciences*, Vol. 51, No. 3, 2003, pp. 279-290.
- [14] Ahmed, J., Coppola, V., and Bernstein, D., "Adaptive Asymptotic Tracking of Spacecraft Attitude Motion with Inertia Matrix Identification," *Journal of Guidance, Control, and Dynamics*, Vol. 21, No. 5, 1998, pp. 684-691. doi:10.2514/2.4310
- [15] Chaturvedi, N. A., Bernstein, D. S., Ahmed, J., Bacconi, F., and McClamroch, N. H., "Globally Convergent Adaptive Tracking of Angular Velocity and Inertia Identification for a 3-DOF Rigid Body," *IEEE Transactions on Control Systems Technology*, Vol. 14, No. 5, 2006, pp. 841-853. doi:10.1109/TCST.2006.876908
- [16] Thienel, J., Luquette, R., and Sanner, R., "Estimation of Spacecraft Inertia Parameters," AIAA Guidance, Navigation and Control Conference and Exhibit, Honolulu, HI, AIAA Paper 2008-6454, Aug. 2008. pp. 1-8. doi:10.2514/6.2008-6454
- [17] Leve, F. and Jah, M., "Spacecraft actuator alignment determination through null-motion excitation," *IEEE Transactions on Aerospace and Electronic Systems*, Vol. 50, No. 3, 2014, pp. 2336-2342. doi:10.1109/TAES.2013.120187
- [18] Bergmann, E. V., Walker, B. K., and Levy, D. R., "Mass Property Estimation for Control of Asymmetrical Satellites," *Journal of Guidance, Control, and Dynamics*, Vol. 10, No. 5, 1987, pp. 483-491. doi:10.2514/3.20243
- [19] Psiaki, M. L., Klatt, E. M., Kintner Jr., P. M., and Powell, S. P., "Attitude Estimation for a Flexible Spacecraft in an Unstable Spin," *Journal of Guidance, Control, and Dynamics*, Vol. 25, No. 1, 2002, pp. 88-95. doi:10.2514/2.4853
- [20] Psiaki, M. L., "Global Magnetometer-Based Spacecraft Attitude and Rate Estimation," *Journal of Guidance, Control, and Dynamics*, Vol. 27, No. 2, 2004, pp. 240-250. doi:10.2514/1.1039
- [21] Psiaki, M. L., "Estimation of a Spacecraft's Attitude Dynamics Parameters by Using Flight Data," *Journal of Guidance, Control, and Dynamics*, Vol. 28, No. 4, 2005, pp. 594-603. doi:10.2514/1.7362
- [22] Fosbury, A. M. and Nebelecky, C. K., "Spacecraft Actuator Alignment Estimation," AIAA Guidance, Navigation, and Control Conference, Chicago, IL, AIAA Paper 2009-6316, Aug. 2009, pp. 1-18. doi:10.2514/6.2009-6316
- [23] Norman, M. C., Peck, M. A., and Shaughnessy, D. J., "In-orbit estimation of inertia and momentum actuator alignment parameters," *Journal of Guidance, Control, and Dynamics*, Vol. 34, No. 6, 2011, pp. 1798-1814. doi:10.2514/1.53692
- [24] Pittelkau, M., "RIMU Misalignment Vector Decomposition," AIAA/AAS Astrodynamics Spe-

cialist Conference and Exhibit, Providence, RI, AIAA Paper 2004-4856, Aug. 2004, pp. 1-9.
doi:10.2514/6.2004-4856

[25] Schrello, D. M., "Passive aerodynamic attitude stabilization of near Earth satellites. volume I. Libra-
tions due to combined aerodynamic and gravitational torques," No. WADD-TR-61-133. North America
Aviation Inc., Columbus, Ohio, 1961.

[26] Wie, B., Weiss, H., and Arapostathis, A., "Quartenion Feedback Regulator for Spacecraft Eige-
naxis Rotations," *Journal of Guidance, Control, and Dynamics*, Vol. 12, No. 3, 1989, pp. 375-380.
doi:10.2514/3.20418

[27] Julier, S., Uhlmann, J., and Durrant-Whyte, H. F., "A New Method for the Nonlinear Transformation
of Means and Covariances in Filters and Estimators," *IEEE Transactions on Automatic Control*, Vol.
45, No. 3, 2000, pp. 477-482. doi:10.1109/9.847726

[28] Crassidis, J. and Markley, F. L., "Unscented Filtering for Spacecraft Attitude Estimation," *Journal of
Guidance, Control, and Dynamics*, Vol. 26, No. 4, 2003, pp. 536-542. doi:10.2514/2.5102

[29] Marlow, W. A. N., "Improving attitude determination and control of resource-constrained CubeSats
using unscented Kalman filtering," S.M. Thesis, Massachusetts Institute of Technology, 2016.

[30] Gerhardt, D. T. and Palo, S. E., "Passive Magnetic Attitude Control for CubeSat Spacecraft," *Proceed-
ings of the AIAA/USU Conference on Small Satellites*, Student Competition, SSC10-VII-5, 2010.

[31] Rawashdeh, S. A. and Lumpp, J. E., "Aerodynamic Stability for CubeSats at ISS Orbit," *Journal of
Small Satellites*, Vol. 2, No. 1, 2013, pp. 85-104.

[32] Franquiz, F. J., Edwards, P., Udrea, B., Nayak, M. V., and Pueschl, T., "Attitude Determination
and Control System Design for a 6U CubeSat for Proximity Operations and Rendezvous," AIAA/AAS
Astrodynamics Specialist Conference, San Diego, CA, AIAA Paper 2014-4421, Aug. 2014, pp. 1-19.
doi:10.2514/6.2014-4421